A global model for fast calculation of the thermal response factor of large-scale boreholes heat exchangers combining the FLS model, the 2D heat equation and a threepoints method

Long Pei, Patrick Schalbart, Bruno Peuportier

A global model for fast calculation of the thermal response factor of large-scale boreholes heat exchangers combining the FLS model, the 2D heat equation and a three-points method

Long PEI [1], Patrick SCHALBART[1], Bruno PEUPORTIER[1]
[1] MINES ParisTech, PSL Research University, CES - Centre d'efficacité énergétique des systèmes, 60 Bd St Michel 75006 Paris, France

Abstract

In order to progress towards more energy efficient buildings, vertical ground coupled heat pumps are a promising solution. Optimisation of both the design and operation of boreholes heat exchangers is a key factor to reduce energy consumption of such systems. This requires a fast evaluation of the thermal response factor of the ground heat exchanger, particularly if it contains numerous boreholes and operates for multiple years. To overcome this challenge, this article reports a new global model combining the finite line source (FLS) model, the two-dimensional (2D) heat conduction equation, and a newly developed three-points method. The borehole field is sorted in increasing distance categories, each being simulated with varying timesteps. The 2D heat conduction equation is used to determine: 1) when the detailed calculation needs to be performed; and 2) the growth of the timestep. A three-points method avoiding double integration of the temperature profiles is proposed to evaluate the borehole wall temperature. The global model calculation time and accuracy were evaluated. The thermal response factor calculation for a square field of 26×26 boreholes for 1 simulated year took 4 seconds, showing a calculation time reduction factor of around 1 000 000, and relative errors smaller than 2 % compared to the original FLS model with superposition principle. For 20 simulated years, the proposed model took only 1 minute. It is appropriate for various boreholes configurations. Its features such as accuracy, speed and load-independency are essential for its integration into building energy simulation tools.

Keywords: geothermal boreholes; ground heat exchanger; thermal response factor; finite line source; two-dimensional heat equation; calculation time reduction

1 . Introduction

Vertical ground coupled heat pump (GCHP) systems have been more and more widely used in the buildings sector in China because of their energy efficiency [1] and environmental friendliness [2]. A vertical GCHP system mainly consists of a vertical ground heat exchanger (GHE), heat pumps and distribution units. The vertical GHE exchanges heat with the ground that serves as a heat source or heat sink, respectively in winter and summer. Buildings might be equipped with large-scale boreholes GHEs which may contain hundreds of boreholes due to their high energy loads [3]. The optimisation of the design and control of GCHP systems can yield more energy efficient buildings [4]. A building energy simulation (BES) tool integrated with a vertical GCHP model is helpful for building designers to achieve this goal. However, it is difficult and time costing due to the large amount of calculations required for a large-scale boreholes GHE.

The simulation of a GHE mainly aims at predicting its returning fluid temperature and the ground temperature in the borehole field [5]. Fast and accurate calculation of these temperatures is essential for the long-term evaluation of the GCHP performance and the proper design of the system [6,7]. The temperature variation of a point in the ground can be represented in a dimensionless form by introducing a proper thermal response factor (also called temperature response factor in some references [8–10]), which gives the relation between the temperature variation and the overall heat extraction rate in the borehole field. The most utilised method to analyse a vertical GHE consisting of large-scale boreholes is firstly to use a heat transfer model of a single borehole to obtain the thermal response factor of one borehole, and secondly to apply Duhamel's superposition principle [11] to evaluate the temperature responses caused by all the boreholes in the field [12].

The energy analysis models for one borehole can be divided into analytical models and numerical models. Although the numerical models [13–19] might take into account all the elements (including U-pipe, grout and ground) and offer more accurate results compared to analytical models using

simplifying assumptions [20], they are very complex and they cannot be easily integrated into BES tools. Many analytical models have been proposed [21] such as the infinite line source model [22], the finite line source (FLS) model [23], the infinite cylinder source model [24], the infinite composite-medium line source method [25], the full scale model [26], and the transient quasi-3D entire time scale line source model [27]. These analytical models are more easily implemented in BES tools. The FLS model is widely employed in GHE simulation for its simple mathematical form and relatively good accuracy in long operation time simulation, therefore this study is based on this model. Some studies improved the FLS model by considering more elements, such as multilayer [28], heat fluxes at the ground surface [29], buried depth [30], advection of vertical water flow [31] and more complex initial and boundary conditions [32]. As a first step and in order to present our model more easily and clearly, this article focuses on the original FLS model. These improvements could be integrated in future work.

The borehole wall temperature is an essential parameter in the borehole analytical model. The outlet fluid temperature of a borehole could be derived if the borehole wall temperature is known, and thus the outlet fluid temperature of the whole borehole field. In Zeng et al.'s study [23], it is indicated that the middle-point temperature (called the middle-point method in this paper) and the integral mean temperature (called the double-integration method in this paper) could be two representative borehole wall temperatures in the FLS model, and that the middle-point temperature is more often chosen for its convenience. However, there are two main problems for the application of this method. The first problem is the conflict between accuracy and calculation speed of the FLS model. If the middle-point temperature is used to represent the borehole wall temperature, the accuracy can be low when the operation time is long (section 3.2) [33]. If the integral mean temperature is used, the double-integration form of the model (see equation (2) in section 2.1) increases the calculation complexity [34]. The second problem is that the calculation load is massive when a large-scale borehole field operates over a long time (e. g. a 26×26 borehole field during 20 years) under dynamic loads. Long time scales (larger amount of data), varying loads (thermal history) and multiple boreholes (thermal interactions) are the three major challenges to obtain the optimal design of GHEs based on the operating performance simulation of GCHPs [35]. The intensive computation makes this method not suited to be integrated into BES tools.

A few studies have been conducted to simplify the calculation for a large-scale boreholes GHE operating for a long period. Yavuzturk and Spitler [36] proposed the load-aggregation algorithm to lump the hourly loads on GHEs into larger blocks of time. Cullin and Spitler [37] proposed a computationally efficient hybrid time-step methodology for simulation of GHEs by setting a reasonable peak load and peak load duration according to the daily load profiles. Bernier et al. [38] presented a multiple load aggregation algorithm to perform annual hourly energy simulations, by subdividing the past thermal history into four time intervals. Claesson and Javed [39] proposed a new load-aggregation scheme to perform multi-year simulations of GHEs using a step-response function. Mitchell and Spitler [40] investigated the different parameters in the developed load aggregation methods and claimed a 73-fold reduction in simulation time when compared to non-aggregated simulations. However, the computed hourly temperature is not exactly that corresponding to the heat load history obtained by the load-aggregation algorithm [35]. The reshaping of load history does not simulate the interactions between the ground temperature and the heat pump efficiency at each timestep which is an important feature for the integration in the BES tools. Lamarche and Beauchamp [41] presented a history-independent mathematical algorithm to calculate ground dynamic thermal response by applying Green function to solve heat conduction problem of the infinite cylinder source model. It can be applied in GHEs under any kind of step response [42]. Zhang et al. [43] used the fast Fourier transform (FFT) method to reduce computational complexity but did not provide a detailed description. Marcotte and Pasquier [44] proposed a method to reduce the computing time by sub-sampling the analytical function at a few selected times with a geometric sequence using the cubic spline interpolant, and based on FFT. Katsura et al. [44] presented a high-speed algorithm to calculate the ground temperature of multiple GHEs, reducing the computation time by about a factor 135. Zhang [46] indicated that a representative boreholes matrix of 3×3 can be employed to substitute the large-scale boreholes GHEs based on his study for a GHE operating for dozens of days. However this representative boreholes matrix is not appropriate for longer operation time. Chen et al. [6] combined

a δ-function (a thermal response factor to unit rectangular heat pulse) with FFT; it took only less than 1.5 minutes for a 30-years hourly simulation of 5 × 8 boreholes. Some researchers [47,48] used monthly loads to simulate long term operation to avoid long calculation time. Beck et al. [49] divided a rectangle borehole field into four mirror symmetric quadrants so the calculation time can be reduced to one fourth, but even a single month by month load for a period of 30 years still required a calculation time of several minutes. Yu et al. [12] indicated that a representative boreholes matrix can replace the original large-scale ground heat exchanger for heat transfer analysis and proposed the method to determine the number of the representative boreholes matrix from the thermal influence radius of a single borehole. This method indeed reduces calculation complexity by using geometric simplification but still cannot solve the difficulty of the large computing resources needed when the operation time is long. Cimmino and Bernier [50] introduced a new methodology for the generation of thermal response factors of geothermal borehole fields. They proposed to divide boreholes into segments to consider the variation of the heat extraction rates along the length of the boreholes. However this method will increase the calculation time. Then, Cimmino [7] introduced a similarity identification method and a load history reconstruction method for fast calculation. The similarity identification method identifies the pairs of boreholes that have the same FLS calculation value, and the load history reconstruction method evaluates the thermal response factors at non-uniform timesteps. The calculation time for the *g*-function of a rectangular field of 12 × 12 boreholes is reduced by a factor 300.

It can be inferred from the literature review that although some efforts have been made on reducing the computation load, there is still a lack of a global, convenient and fast model to simulate the large-scale boreholes GHE, especially one which can be easily linked with GCHP models and integrated into a BES tool without reshaping the load history. This article presents a new global model, which is different from the existing methods, that overcomes the abovementioned issues. The main goal of this work is to propose a fast calculation method for the thermal response factor based on the FLS model. Firstly, the GHE model is introduced by using the FLS model and the superposition method. Secondly, a novel method (the three-points method) to evaluate the borehole wall temperature is presented. Thirdly, a new model to quickly calculate the thermal response factor of the large-scale boreholes GHE is proposed, combining the FLS model, the two-dimensional (2D) heat equation and the three-points method, and then applied to a case study. Finally, the model is validated against the original FLS model, and the results are presented and discussed. It should be noted that in this paper, if not particularly indicated, the time refers to the operation time of a borehole or a GHE from initial conditions where the ground temperature is uniform.

2 . GHE heat transfer model

2.1 Finite line source model

In the FLS model, the ground is regarded as a homogeneous semi-infinite medium with constant thermophysical properties and a uniform initial temperature. The effects of underground water, air temperature variations and solar radiation are not taken into consideration. The radial dimension of the borehole is neglected so that it may be approximated as a line-source stretching from the ground surface to the borehole depth.

Considering the effects of one borehole exchanging heat with the ground at a constant heat load q (positive values when a GHE extracts heat from the ground), the ground temperature T at any point at time t, as shown in Figure 1, is given by the FLS model [23]:

$$T(r,z,t)-T_0=\frac{-q}{2\pi\lambda_s}\cdot\frac{1}{2}\int_0^H\left\{\frac{\operatorname{erfc}\left(\frac{\sqrt{(r)^2+(z-h)^2}}{2\sqrt{\alpha_s t}}\right)}{\sqrt{(r)^2+(z-h)^2}}-\frac{\operatorname{erfc}\left(\frac{\sqrt{(r)^2+(z+h)^2}}{2\sqrt{\alpha_s t}}\right)}{\sqrt{(r)^2+(z+h)^2}}\right\}\mathrm{d}h=\frac{-q}{2\pi\lambda_s}\,G(r,t,z) \tag{1}$$

where r is the radial distance to the borehole centre line; z is the vertical coordinate; T_0 is the initial ground temperature; λ_s and α_s are respectively the thermal conductivity and thermal diffusivity of the

ground; H is the borehole depth; h is an integral variable along borehole depth; G is the thermal response factor; and erfc denotes the complementary error function.

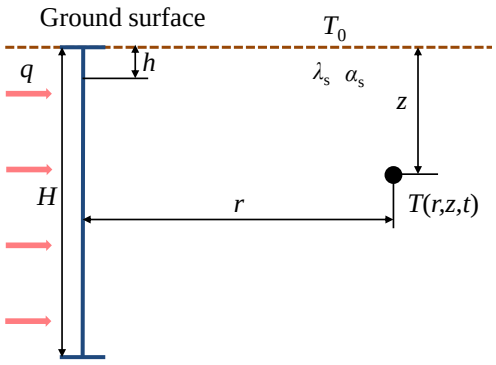

Figure 1: Temperature in the ground under the effect of one borehole

The integral mean temperature along the borehole length is considered to be a reasonable proxy to represent the borehole temperature [23], which can be obtained by the double-integration method. Thus, considering the heat interaction between two boreholes, the borehole wall temperature T_b of a borehole at time t under the effect of the other borehole located at radial distance r with constant heat load q is given by:

$$T_b(r,t) - T_0 = \frac{-q}{2\pi\lambda_s}\frac{1}{2H}\int_0^H\int_0^H \left\{ \frac{\operatorname{erfc}\left(\frac{\sqrt{(r)^2+(z-h)^2}}{2\sqrt{\alpha_s t}}\right)}{\sqrt{(r)^2+(z-h)^2}} - \frac{\operatorname{erfc}\left(\frac{\sqrt{(r)^2+(z+h)^2}}{2\sqrt{\alpha_s t}}\right)}{\sqrt{(r)^2+(z+h)^2}} \right\} \mathrm{d}h\,\mathrm{d}z \tag{2}$$

$$= \frac{-q}{2\pi\lambda_s} G_{2i}(r,t)$$

where $G_{2i}(r,t)$ is the thermal response factor of a borehole wall temperature under the other borehole's effect using the double-integration method. Considering a special case for the self-effect of one borehole, the borehole wall temperature response under the effect of its own heat load can be calculated by setting $r = r_b$, where r_b is the borehole radius.

2.2 Superposition principle

In the BES model COMFIE developed by Peuportier's research group [51], the time-varying heating and cooling loads are step-wise constant values. Even though some studies (e.g. [52]) suggest considering the non-uniform distribution of the energy load of the building to each borehole, here a uniform distribution is assumed. It corresponds to the first type of boundary condition defined in [50] and it is a common assumption adopted for multiple borehole heat exchangers [12,53–55]. This assumption is made because this work mainly aims at fast calculation of G_{2i}, which is a dimensionless response factor independent from the energy load. The uniform distribution could help simplify the mathematics regarding the temperature. This will be discussed in more detail in section 4.5. However the non-uniform distribution of the heating load for each borehole could be an improvement of this method. Therefore, the heat loads of all boreholes during a timestep are identical:

$$q_{1,m} = q_{2,m} = \cdots = q_{i,m} = \cdots = q_{N_b,m} = q_m = \frac{Q_{GHE}(m)}{N_b \times H} \tag{3}$$

$q_{i,m}$ is the lineic heat load of i^{th} boreheole in a GHE consisting of N_b identical boreholes at timestep m; q_m is the lineic heat load of a single borehole; and $Q_{GHE}(m)$ is the heat load of the GHE field at timestep m.

The borehole wall temperature in a large-scale boreholes GHE could be evaluated by employing the superposition principle to the FLS model. The superposition principle consists of the temporal superposition and spatial superposition. The time-varying heating and cooling loads are step-wise constant values in this study, as shown in Figure 2 (a). In fact, the heat load has an effect on both the current time and the future, as shown in Figure 2 (b). For one borehole without the effects of other boreholes, its borehole wall temperature at timestep m is determined by employing temporal superposition to equation (2):

$$T_{\mathrm{b}}(t_m) - T_0 = \sum_{k=1}^{m} \frac{q_{k-1} - q_k}{2\pi\lambda_{\mathrm{s}}} \frac{1}{2H} \int_0^H \int_0^H \left\{ \frac{\operatorname{erfc}\left(\frac{\sqrt{(r_{\mathrm{b}})^2 + (z-h)^2}}{2\sqrt{\alpha_{\mathrm{s}}(t_m - t_{k-1})}} \right)}{\sqrt{(r_{\mathrm{b}})^2 + (z-h)^2}} - \frac{\operatorname{erfc}\left(\frac{\sqrt{(r_{\mathrm{b}})^2 + (z+h)^2}}{2\sqrt{\alpha_{\mathrm{s}}(t_m - t_{k-1})}} \right)}{\sqrt{(r_{\mathrm{b}})^2 + (z+h)^2}} \right\} \mathrm{d}h\, \mathrm{d}z \tag{4}$$

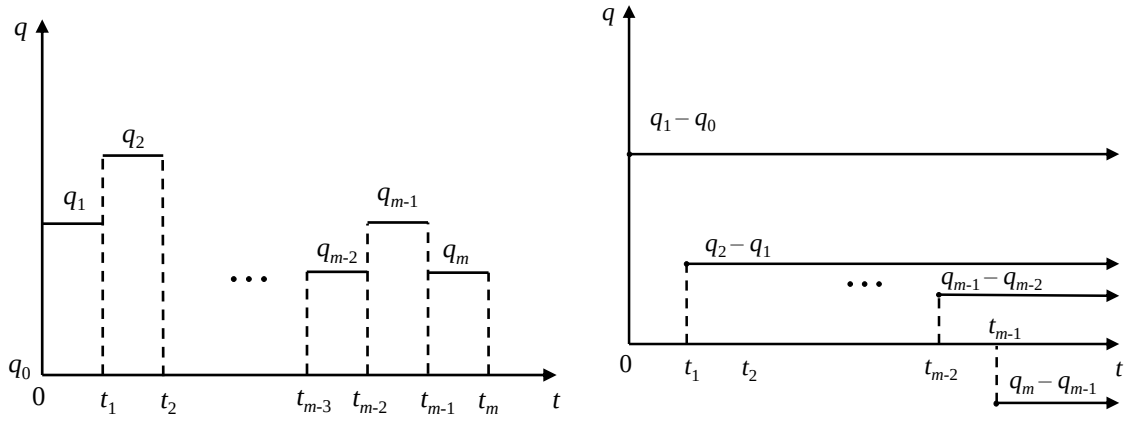

Figure 2: Temporal superposition principle for the timesteps of one borehole heat load: (a) the step-wise heat load and (b) heat load increment for various time intervals

The spatial superposition considers the effects of other boreholes on the calculated borehole, as shown in Figure 3. The borehole wall temperature of the j^{th} borehole at timestep m can be determined by applying the spatial superposition to equation (4):

$$T_{\mathrm{b},j}(t_m) - T_0 = \sum_{i=1}^{N_{\mathrm{b}}} \sum_{k=1}^{m} \frac{q_{k-1} - q_k}{2\pi\lambda_{\mathrm{s}}} \frac{1}{2H} \int_0^H \int_0^H \left\{ \frac{\operatorname{erfc}\left(\frac{\sqrt{(r_{i,j})^2 + (z-h)^2}}{2\sqrt{\alpha_{\mathrm{s}}(t_m - t_{k-1})}} \right)}{\sqrt{(r_{i,j})^2 + (z-h)^2}} - \frac{\operatorname{erfc}\left(\frac{\sqrt{(r_{i,j})^2 + (z+h)^2}}{2\sqrt{\alpha_{\mathrm{s}}(t_m - t_{k-1})}} \right)}{\sqrt{(r_{i,j})^2 + (z+h)^2}} \right\} \mathrm{d}h\, \mathrm{d}z \tag{5}$$

$$= \sum_{i=1}^{N_{\mathrm{b}}} \sum_{k=1}^{m} \frac{q_{k-1} - q_k}{2\pi\lambda_{\mathrm{s}}} G_{2\mathrm{i}}(r_{i,j}, t_m - t_{k-1})$$

where i is the i^{th} borehole in the borehole field; k is the k^{th} timestep; q_k is the heat load of each boreheole at timestep k; $r_{i,j}$ is the radial distance between borehole centre lines of i^{th} boreheole and j^{th} boreheole, and $r_{i,j} = r_{\mathrm{b}}$ when $i = j$; t_m is the time at timestep m.

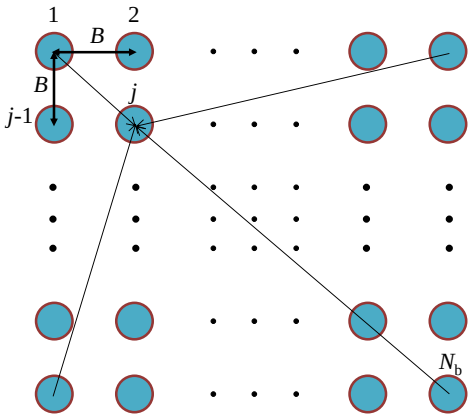

Figure 3: A square borehole field consisting N_b boreholes and the spatial superposition principle

2.3 Modelling challenges for large-scale boreholes GHE

Equation (5) shows that the calculation of one borehole wall temperature can be costly due to three challenges: (1) its double-integration form, (2) the interactions with a large number of boreholes N_b, and (3) the calculation of G for a large number of timesteps m. Besides, the calculation load of the GHE needs to be multiplied by a factor of N_b because this calculation needs to be performed for each borehole, which brings the final challenge: (4) to model the large-scale boreholes GHE in the BES tools. Thus, a global model is presented in the following section to solve these issues.

3 . Global model for fast calculation of thermal response factor

3.1 Case description

To illustrate the proposed model, a case study is introduced in Table 1, assuming that the ground is siliceous rock [56]. For the sake of simplificity for the presentation of the methods, a constant heat flux q of 10 W/m is assumed, considering a yearly unbalanced heating and cooling load [23]. In the BES tools, the load is variable and therefore the temporal superposition should be considered. The default duration of one timestep is 1 hour, but it can be changed as needed.

Table 1: Main parameters of the case study

Component	Parameter	Value	Unit
GHE	Layout	26 × 26	
	Number of total boreholes N_b	676	
	Borehole spacing B	4	m
	Borehole length H	133	m
	Radius for the borehole r_b	0.11	m
Ground	Ground thermal conductivity λ_s	2.635	W/m.K
	Ground thermal diffusivity α_s	1.23×10^{-6}	m^2/s
	Intial ground temperature T_0	19	°C
Building load	Heat flux q	10	W/m

3.2 Three-points method

By using the middle-point method, the borehole wall temperature T_b of a borehole at time t under the effect of the other borehole located at radial distance r with constant heat load q is given by:

$$T_b(r,t) - T_0 = \frac{-q}{2\pi\lambda_s} \cdot \frac{1}{2} \int_0^H \left\{ \frac{\operatorname{erfc}\left(\frac{\sqrt{(r)^2 + \left(\frac{H}{2} - h\right)^2}}{2\sqrt{\alpha_s t}} \right)}{\sqrt{(r)^2 + \left(\frac{H}{2} - h\right)^2}} - \frac{\operatorname{erfc}\left(\frac{\sqrt{(r)^2 + \left(\frac{H}{2} + h\right)^2}}{2\sqrt{\alpha_s t}} \right)}{\sqrt{(r)^2 + \left(\frac{H}{2} + h\right)^2}} \right\} \mathrm{d}h$$
$$= \frac{-q}{2\pi\lambda_s} G_m(r,t) \tag{6}$$

where $G_m(r,t)$ is the thermal response factor of a borehole wall temperature under the other borehole's effect using the middle-point method.

However, we found that the difference between the middle-point temperature and the integral mean temperature due to the heat flux can be non-negligible. For two typical boreholes with parameters in Table 1, the considered borehole wall temperature differences between the middle-point method and the double-integration method (as reference) under the effect of the other borehole at different radial distances and times are shown in Figure 4 (a). For the self-effect of the borehole ($r = r_b = 0.11$ m), the absolute temperature difference is over 0.1°C when $t \geqslant 5$ years. It increases with time and can reach over 0.2 °C after 25 years. This difference increases with the number of boreholes. Considering the effects of all boreholes, the wall temperature of the borehole located at the corner and in the centre with different sizes of borehole fields is shown in Figure 4 (b) and (c) respectively. It is found that the absolute temperature difference increases with the field size. The difference could reach over 12 °C for the corner borehole and 36 °C for the centre borehole when $t = 25$ years for a 26 × 26 field, which is not acceptable for the fluid temperature calculation. The middle-point method is not appropriate for large borehole fields for long operation time. This non negligible difference was also observed in [33].

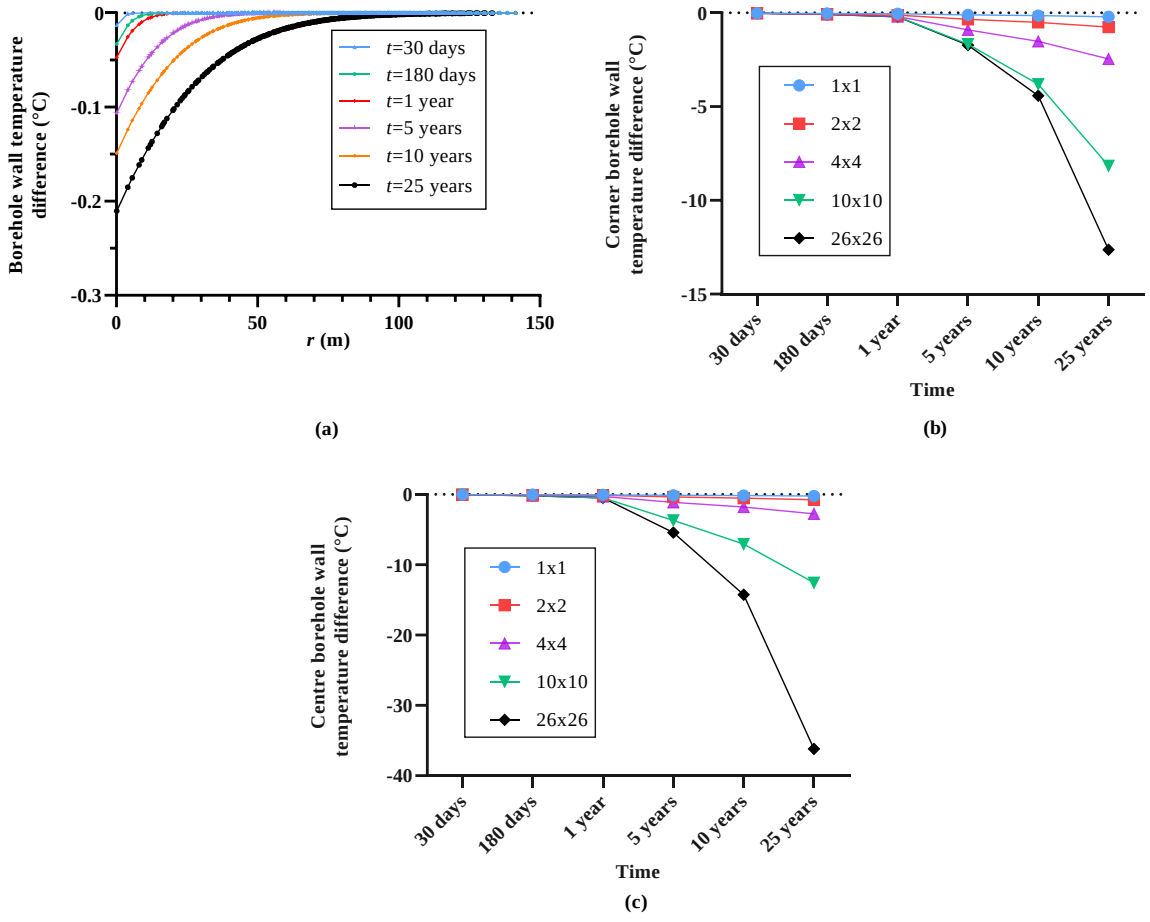

Figure 4: (a) The borehole wall temperature differences under the effect of a single borehole located at radial distance r and the borehole wall temperature difference (b) for the corner borehole and (c) for the centre borehole in a field with different sizes between the middle-point method and the double-integration method (as reference)

The borehole wall temperature evolution under the self-effect with depth at different times is shown in Figure 5 (a). The borehole wall temperature tends to remain constant around the middle. However, it varies sharply at the top and bottom of the borehole due to the finite length of the borehole. Only using the middle-point temperature cannot represent the borehole wall temperature, especially when time is long (beyond 1 year), because it does not consider the top and bottom parts. If the integral mean temperature is used, the single integration will become double integration (see equation (2)) in the

calculation, which will sharply increase the computational time. Thus, a method that gives a good calculation accuracy and keeps the single-integration form is needed.

In the proposed method, three typical points (P_{top}, P_{middle} and P_{bottom}) are chosen instead of only one middle point, as shown in Figure 5 (b), and the average temperature of these three points is used to represent the borehole wall temperature. The three points are the middle point and two points symmetrical to the middle point located in the top and bottom areas, so the effects of the borehole top, middle and bottom can be all taken into consideration. This method is called the three-points method for the borehole wall temperature calculation in this paper.

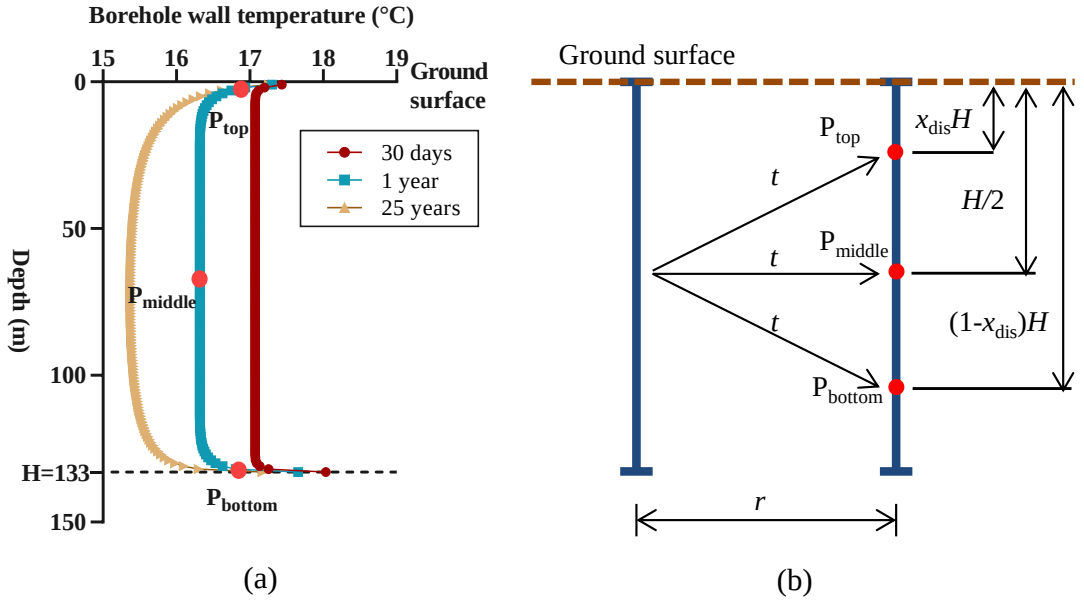

Figure 5: (a) Borehole wall temperature evolution under the self-effect with depth at different times (b) the three-points method to calculate a borehole wall temperature under the other's effect

The top and bottom points are located at H_{top} and H_{bottom} respectively. Although the borehole wall temperature T_b at time t under the effect of another borehole at radial distance r varies with depth, assuming a constant heat load q is a necessary approximation to apply the FLS model. This leads to the following equation:

$$\begin{aligned} T_b(r,t) - T_0 &= \frac{-q}{2\pi\lambda_s} \cdot \frac{1}{3}\{G(r,t,H_{top}) + G(r,t,H/2) + G(r,t,H_{bottom})\} \\ &= \frac{-q}{2\pi\lambda_s} G_{3p}(r,t) \end{aligned} \quad (7)$$

where $H_{top} = x_{dis}H$, $H_{bottom} = (1 - x_{dis})H$; x_{dis} is the location factor of the top point; and $G_{3p}(r,t)$ is the thermal response factor of a borehole wall temperature under the other borehole's effect using the three-points method. It should be noted that the top and bottom points are assumed to be symmetrical in order to keep equation (7) simple. In perspective, these two points could be non-symmetrically located to improve the accuracy.

In order to apply this method, it is essential to determine the location factor x_{dis}. Firstly, we identified the optimal x_{dis} for different radial distances r (0.11 m to 200 m), time t (30 minutes to 25 years) and borehole depths H (20 m to 200 m). Then we assumed that x_{dis} is an exponential function of these three parameters:

$$x_{dis} = \max\left(a_1 + a_2\left(1 - e^{(-a_3 \cdot t)}\right) + a_4\left(1 - e^{(-a_5 \cdot r)}\right) + a_6\left(1 - e^{\left(-\frac{H - a_7}{a_7}\right)}\right), a_8\right) \quad (8)$$

The coefficients a_1 to a_8 were finally obtained by using an exponential regression method ($a_1 = 0.056$, $a_2 = 0.0425$, $a_3 = 8.39 \times 10^{-9}$, $a_4 = 0.0443$, $a_5 = 0.105$, $a_6 = -0.03$, $a_7 = 118.5$). Moreover, x_{dis} was constrained to a minimum ($a_8 = 0.052$). The identification process of these parameters is shown in Appendix A. It should be noted that equation (8) is based on the soil parameters in Table 1. A more general equation covering a larger scale of the parameters should be developed.

Using the three-points method and considering the superposition method, $T_{b,j}(m)$ is given by the single-integration equation below, which solves challenge (1):

$$\begin{aligned} T_{b,j}(t_m) - T_0 = & \sum_{i=1}^{N_b} \sum_{k=1}^{m} \frac{q_{k-1} - q_k}{2\pi\lambda_s} \\ & \cdot \frac{1}{3}\{G(r_{i,j}, t_m - t_{k-1}, x_{dis}H) + G(r_{i,j}, t_m - t_{k-1}, H/2) + G(r_{i,j}, t_m \\ & - t_{k-1}, (1 - x_{dis})H)\} \\ = & \sum_{k=1}^{m} \frac{q_{k-1} - q_k}{2\pi\lambda_s} \sum_{i=1}^{N_b} G_{3p}(r_{i,j}, t_m - t_{k-1}) \end{aligned} \quad (9)$$

3.3 Distance category simplification

For a borehole in a square field of N_b boreholes at a certain timestep as shown in Figure 3, the interactions with other boreholes are calculated based on the radial distance. This requires N_b evaluations of G_{3p}, as shown in equation (9). If it is used to calculate the outlet fluid temperature of the GHE at a certain timestep, G_{3p} will be calculated $N_b \times N_b$ times. However the calculation of G_{3p} at a certain timestep is only a function of the radial distance $r_{i,j}$ between boreholes i and j. Identical radial distances will bring unnecessary repetition of calculation of G_{3p}: for the same $r_{i,j}$, G_{3p} only needs to be calculate once.

Thus, the idea of distance category simplification is to identify all the possibilities of $r_{i,j}$ (entitled distance category in the following, each distance category corresponds to a specific radial distance), and calculate the corresponding G_{3p}. Then, in order to calculate each borehole's wall temperature, only the number of times each distance category occurs needs to be identified (that is the number of times other boreholes located at the radial distance from the considered borehole are found); afterwards the accumulation needs to be performed to determine G_{3p} for each distance category. For a square field of N_b boreholes, there exist N_d radial distance possibilities in total. The number of times G_{3p} evaluated is reduced by a factor $\frac{N_b \times N_b}{N_d}$, which is a significant calculation time reduction. A similar idea is also found in other references e.g. [57].

An example of a square 3×3 borehole field is shown in Figure 6. There exist 5 radial distance possibilities between a pair of boreholes: B, $\sqrt{2}B$, $2B$, $\sqrt{5}B$ and $\sqrt{8}B$. Considering the radial distances between borehole 1 and the other boreholes, B occurs twice: from 1 to 2 and from 1 to 3; $\sqrt{2}B$ occurs once: from 1 to 5; $2B$ occurs twice: from 1 to 3 and from 1 to 7; $\sqrt{5}B$ occurs twice: from 1 to 6 and from 1to 8; $\sqrt{8}B$ occurs once: from 1 to 9. Combining the self-effect, the borehole wall temperature of borehole 1 under all boreholes' effects at timestep m is given by:

$$\begin{aligned} T_{b,1}(t_m) - T_0 = & \sum_{k=1}^{m} \frac{q_{k-1} - q_k}{2\pi\lambda_s} (G_{3p}(r_b, t_m - t_{k-1}) + 2 \cdot G_{3p}(B, t_m - t_{k-1}) \\ & + G_{3p}(\sqrt{2}B, t_m - t_{k-1}) + 2 \cdot G_{3p}(2B, t_m - t_{k-1}) + 2 \cdot G_{3p}(\sqrt{5}B, t_m - t_{k-1}) \\ & + G_{3p}(\sqrt{8}B, t_m - t_{k-1})) \end{aligned} \quad (10)$$

Similarly, other boreholes' temperatures can be derived from the number of times each radial distance occurs.

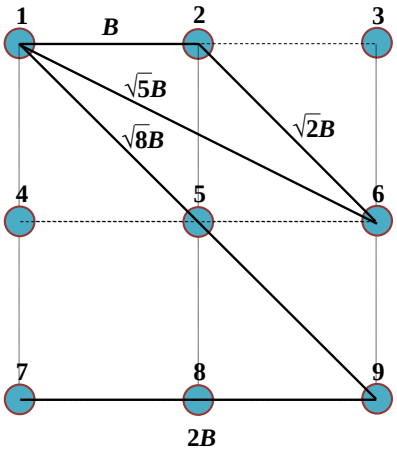

Figure 6: Radial distance possibilities between boreholes in a square 3 × 3 borehole field

For a square field, the radial distances between borehole 1 and the other boreholes contain all possible radial distances between any pair of boreholes in the field. The first step of this distance category simplification method is to calculate $r_{1,j}$ from $j = 1$ to $j = N_b$, and identify and sort them into N_d categories of increasing radial distances. Then for the calculated borehole j, all the boreholes in the field can be converted to N_d categories, as shown in Figure 7, where r_n is the radial distance of the n^{th} distance category, $N_{j,n}$ is the number of times the distance category n occurs for borehole j. The next step is to count $N_{j,n}$ from $j = 1$ to $j = N_b$ and from $n = 1$ to $n = N_d$.

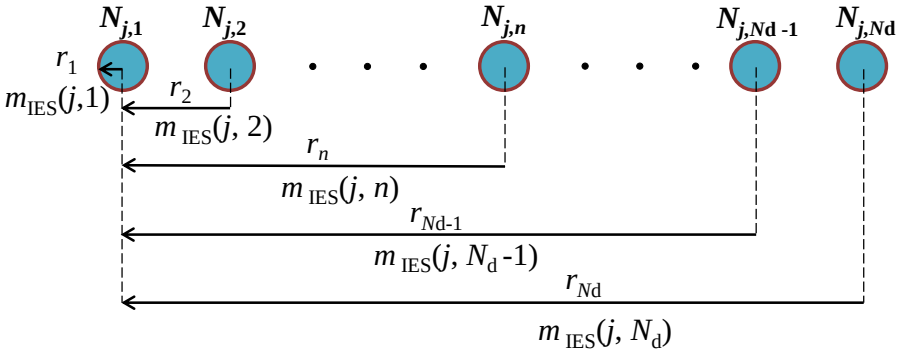

Figure 7: Borehole field converted to distance categories from borehole j

By knowing all $N_{j,n}$, equation (9) can be converted to the following equation, which helps in solving challenge (2):

$$T_{b,j}(t_m) - T_0 = \sum_{k=1}^{m} \frac{q_{k-1} - q_k}{2\pi\lambda_s} \sum_{n=1}^{N_d} N_{j,n} \cdot G_{3p}(r_n, t_m - t_{k-1}) = \sum_{k=1}^{m} \frac{q_{k-1} - q_k}{2\pi\lambda_s} G_{3p,borehole}(j, t_m - t_{k-1}) \quad (11)$$

where $G_{3p,borehole}(j,t_m - t_{k-1})$ is the thermal response factor of j^{th} borehole's wall temperature under all boreholes' effects at time $t_m - t_{k-1}$ using the three-points method.

3.4 Thermal response factor of the GHE

The thermal response factor of the whole GHE at timestep m using the three-points method is given by:

$$G_{3p,GHE}(t_m) = \frac{1}{N_b} \sum_{j=1}^{N_b} G_{3p,borehole}(j, t_m) \quad (12)$$

Similarly, the thermal response factors of the j^{th} borehole's wall temperature under all boreholes' effects and the whole GHE at timestep m using the middle-point method and double-integration method are:

$$G_{\mathrm{m,borehole}}(j,t_m)=\sum_{n=1}^{N_\mathrm{d}} N_{j,n}\cdot G_\mathrm{m}(r_n,t_m) \tag{13}$$

$$G_{\mathrm{2i,borehole}}(j,t_m)=\sum_{n=1}^{N_\mathrm{d}} N_{j,n}\cdot G_\mathrm{2i}(r_n,t_m) \tag{14}$$

$$G_{\mathrm{m,GHE}}(t_m)=\frac{1}{N_\mathrm{b}}\sum_{j=1}^{N_\mathrm{b}} G_{\mathrm{m,borehole}}(j,t_m) \tag{15}$$

$$G_{\mathrm{2i,GHE}}(t_m)=\frac{1}{N_\mathrm{b}}\sum_{j=1}^{N_\mathrm{b}} G_{\mathrm{2i,borehole}}(j,t_m) \tag{16}$$

3.5 Initial effect simplification

The next step is to consider how to simplify the calculation of $G_{3\mathrm{p}}$ for numerous timesteps. The evolution of $G_{3\mathrm{p}}$ with time is presented in Figure 8 for different radial distances during one year. There are two potential methods to reduce the computational complexity: the initial effect simplification (IES) and the time averaging simplification (TAS).

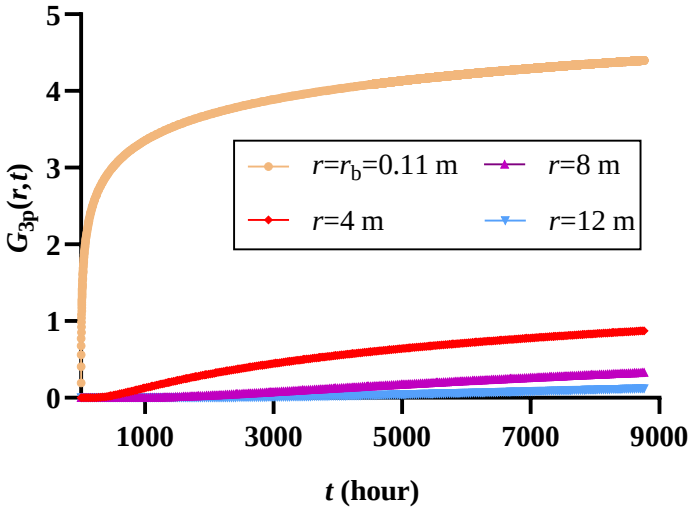

Figure 8: G_{3p} vs t for different r

According to Figure 8, at a certain time, t, the larger r is the smaller $G_{3\mathrm{p}}$ is. This means that for one borehole, the closer the other boreholes, the larger influence they have. Before t = 500 h, $G_{3\mathrm{p}}$ is nearly 0 when r equals to 4 m, 8 m and 12 m. Only the borehole itself ($r = r_\mathrm{b}$ = 0.11 m) has an effect on its wall temperature. That is to say the effects of other boreholes do not reach the considered borehole wall before this time. The further the other borehole, the later it starts to affect the considered borehole. The $G_{3\mathrm{p}}$ calculations concerning all the other boreholes are not necessary because they are negligible. As time goes on, more and more boreholes need to be taken into consideration.

For a field converted to distance categories as presented above, other boreholes located at distance category n start to have a non-negligible effect on borehole j from timestep $m_{\mathrm{IES}}(j,n)$ onwards. $m_{\mathrm{IES}}(j,n)$ is the first timestep that fulfils the following condition:

$$\frac{\sum_{i=1}^{n} N_{j,i}\cdot G_{3\mathrm{p}}(r_i,t_{m_{\mathrm{IES}}(j,n)})}{\sum_{i=1}^{N_\mathrm{d}} N_{j,i}\cdot G_{3\mathrm{p}}(r_i,t_{m_{\mathrm{IES}}(j,n)})}<1-\varepsilon_{\mathrm{IES}} \tag{17}$$

where $\varepsilon_{\mathrm{IES}}$ is the tolerance of the IES method, which is set at 0.5 % in this article. For borehole j, before timestep $m_{\mathrm{IES}}(j,n)$, the effects of distance categories 1 to n - 1 contribute to over 1 - $\varepsilon_{\mathrm{IES}}$ (99.5 %) of the total effect of all distance categories. Figure 7 illustrates how the IES fits into distance categories.

For different boreholes, $m_{\mathrm{IES}}(j,n)$ is different due to the different distance category distribution. In order to simplify the calculations, the minimal $m_{\mathrm{IES}}(j,n)$ among all boreholes is chosen to represent the m_{IES} for distance category n (this conservative approach ensures that the tolerance is respected for all boreholes):

$$m_{\mathrm{IES}}(n) = \min_{1 \le j \le N_{\mathrm{b}}} m_{\mathrm{IES}}(j,n) \tag{18}$$

In fact, only approximately 1/8 of the total boreholes (in total $N_{\mathrm{b,sym}}$) need to be considered due to the symmetry of the squared field, as shown in Figure 9. The idea of symmetry can help in solving challenge (4). Equation (18) can then be converted to:

$$m_{\mathrm{IES}}(n) = \min_{1 \le j \le N_{\mathrm{b,sym}}} m_{\mathrm{IES}}(j,n) \tag{19}$$

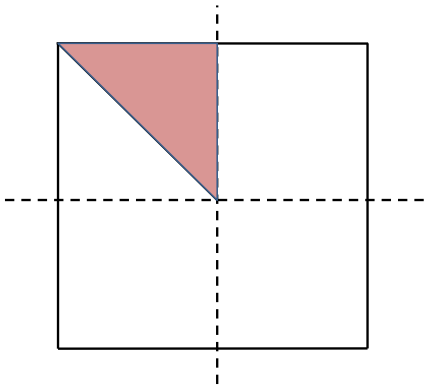

Figure 9: The calculated part (in red) of a square borehole filed after symmetry simplification

Before this timestep $G_{3\mathrm{p}}(r_n,t)$ is negligible, and is therefore set at 0. This method is entitled initial effect simplification method and it can be expressed in the flowing equation:

$$G_{3\mathrm{p}}(r_n,t) = \begin{cases} 0 & if\ t < t_{m_{\mathrm{IES}}(n)} \\ G_{3\mathrm{p}}(r_n,t) & if\ t \gg t_{m_{\mathrm{IES}}(n)} \end{cases} \tag{20}$$

where $t_{m_{\mathrm{IES}}(n)}$ is the time at timestep $m_{\mathrm{IES}}(n)$.

The IES method solves challenge (2) regarding the interactions between boreholes. It determines from which timestep a borehole at a certain distance starts to influence the calculated borehole; no calculation is needed before this timestep, thus much computing effort is avoided. It should be noted that the determination of m_{IES} requires knowing the values of $G_{3\mathrm{p}}$, which is contrary to our goal to calculate $G_{3\mathrm{p}}$. This problem will be solved by the simplified method to determine m_{IES} presented in section 3.7.

3.6 Time averaging simplification

Figure 8 shows that $G_{3\mathrm{p}}$ increases sharply in the beginning and tends to stay stable as time goes. It can be inferred that the closer to the beginning of the operation, the more detailed calculation is needed. Therefore, it is possible to divide the whole timespan into several periods (called averaging periods). In each averaging period, $G_{3\mathrm{p}}$ only needs to be calculated once every certain number of steps (called averaging ranges), because its variation for a specific radial distance during that time is negligible. For an averaging period p, its corresponding averaging range is l_p. The whole timespan is divided into $p_{\max}$ averaging periods. For example, the time averaging simplification of $G_{3\mathrm{p}}$ at the radius of a borehole during one year is shown in Figure 10. This method is named the time averaging simplification method.

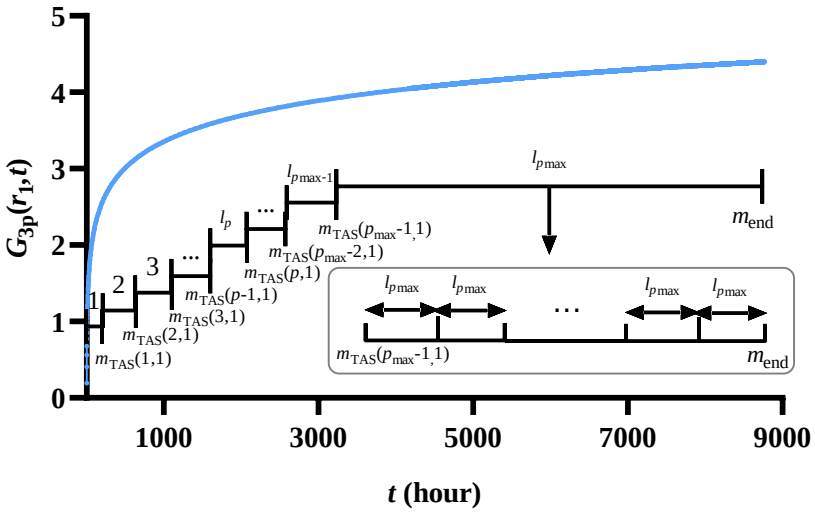

Figure 10: Time averaging simplification method at radial distance r_1

In averaging period 1 (p = 1), G_{3p} is calculated at each timestep (l_1 = 1); in averaging period 2 (p = 2), the averaging range l_2 is 2, is calculated every 2 timesteps; in the last averaging period (averaging period p_{max}), the curve slope is small, so G_{3p} only needs to be calculate every l_{pmax} timesteps. In this paper, the correspondence between p and l_p is set as shown in Figure 11, in which l_{pmax} = 1060, P_{max} = 141.

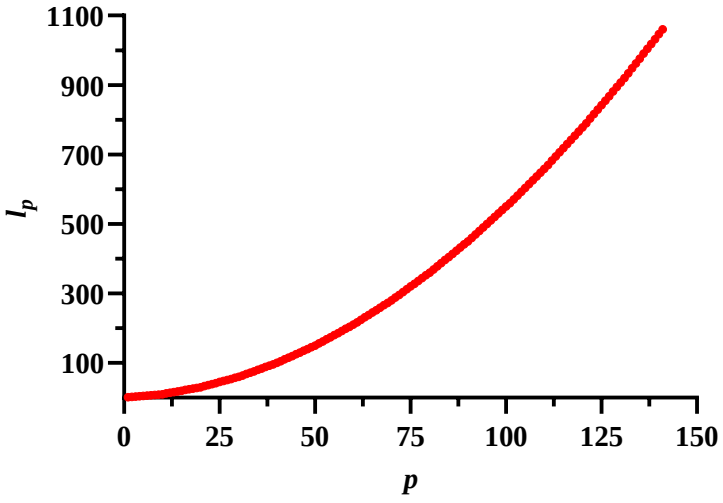

Figure 11: The correspondence between p and l_p

$m_{TAS}(p,n)$ is the timestep at the end of averaging period p for the n^{th} distance category. It is determined by the following three steps:

1. Based on the distance category itself, G_{3p} is used to determine $m_{TAS,dc}(p,n)$ which is the first timestep that fulfils the following condition:

$$\frac{G_{3p}\left(r_n, t_{m_{TAS,dc}(p,n)+l_p}\right) - G_{3p}\left(r_n, t_{m_{TAS,dc}(p,n)}\right)}{\left(G_{3p}\left(r_n, t_{m_{TAS,dc}(p,n)+l_p}\right) + G_{3p}\left(r_n, t_{m_{TAS,dc}(p,n)}\right)\right)/2} < \varepsilon_{TAS} \quad (21)$$

where ε_{TAS} is the tolerance of the time averaging simplification method, which is set at 0.5 % in this study. This equation means that the difference of G_{3p} between the beginning (timestep $m_{TAS,dc}(p,n)$) and the end (timestep $m_{TAS,dc}(p,n) + l_p$) of an averaging range (l_p) within averaging period p is negligible (smaller than 0.5 %). It is used to find $m_{TAS,dc}(p,n)$; G_{3p} only needs to be calculated once every l_p in this averaging period p.

Equation (21) indicates that unlike $m_{\mathrm{IES}}(j,n)$ that depends on the position of the borehole, $m_{\mathrm{TAS,dc}}(p,n)$ is not related to $N_{j,n}$, thus it only needs to be applied to the first borehole which includes all the distance categories.

2. Based on the total effects of all distance categories for one borehole, $G_{\mathrm{3p,borehole}}$ is used to determine $m_{\mathrm{TAS,bh}}(p,j)$ which is the first timestep that fulfils the following condition:

$$\frac{G_{\mathrm{3p,borehole}}\left(j, t_{m_{\mathrm{TAS,bh}}(p,j)+l_p}\right) - G_{\mathrm{3p,borehole}}\left(j, t_{m_{\mathrm{TAS,bh}}(p,j)}\right)}{\left(G_{\mathrm{3p,borehole}}\left(j, t_{m_{\mathrm{TAS,bh}}(p,j)+l_p}\right) + G_{\mathrm{3p,borehole}}\left(j, t_{m_{\mathrm{TAS,bh}}(p,j)}\right)\right)/2} < \varepsilon_{\mathrm{TAS}} \tag{22}$$

Using the symmetry of the square field, the maximal $m_{\mathrm{TAS,bh}}(p,j)$ among all $N_{\mathrm{b,sym}}$ boreholes is chosen to represent m_{TAS} for distance category n (this is conservative to ensure $m_{\mathrm{TAS,bh}}(p,n)$ can cover all the boreholes):

$$m_{\mathrm{TAS,bh}}(p,n) = \max_{1 \le j \le N_{\mathrm{b,sym}}} m_{\mathrm{TAS,bh}}(p,j)\,; n = 1,2,3,\ldots,N_{\mathrm{d}} \tag{23}$$

3. $m_{\mathrm{TAS}}(p,n)$ is the smallest value between $m_{\mathrm{TAS,dc}}(p,n)$ and $m_{\mathrm{TAS,bh}}(p,n)$ (this conservative approach ensures that enough calculations will be done), as shown below:

$$m_{\mathrm{TAS}}(p,n) = \min\left(m_{\mathrm{TAS,dc}}(p,n), m_{\mathrm{TAS,bh}}(p,n)\right) \tag{24}$$

The TAS method solves challenge (3) regarding the numerous calculations of G for long-term simulation by updating its value only when significant change is expected, therefore much calculation time is saved. Similar to m_{IES}, the determination of m_{TAS} also requires knowing the values of G_{3p}. The flowing section 3.7 illustrates how to solve this problem.

3.7 Two-dimensional heat equation

Based on these two simplification methods, G_{3p} does not need to be calculated for each distance category at each timestep. The computation time can be drastically saved. If we want to use the two simplification methods above, the timesteps for simplification (m_{TAS} and m_{IES}) have to be determined before the calculation of G_{3p}. Using equation (17), (21) and (22) to calculate m_{TAS} and m_{IES} requires to firstly calculate G_{3p}, which is contrary to our aim. Therefore, another method is needed to replace G_{3p} in these equations to identify m_{TAS} and m_{IES}.

The 2D heat equation describes how the distribution of heat evolves over time in a solid medium in two dimensions. Considering the axial symmetry, the temperature variation at radial distance r and at time t from uniform initial conditions under a line heat source input at $r = 0$ and $t = 0$ (also called Dirac delta function) is given by [58]:

$$\theta_{\mathrm{he}}(r,t) = \frac{\exp\left(-\frac{r^2}{4\alpha_{\mathrm{s}}t}\right)}{4\alpha_{\mathrm{s}}\pi t} \tag{25}$$

Equation (25) gives the heat propagation under an infinite line source of Dirac delta function, with a simple mathematic form. It represents the theoretical heat propagation speed. Although in this study the borehole is regarded as a finite line source under a step-wise heating load, it can reasonably be represented by equation (25) which in reality, is a conservative approach.

The heat propagation of Dirac delta distribution under different times and radial distances is shown in Figure 12. It takes a certain time for the heat to propagate to a certain radial distance, which is similar to the heat transfer process from a borehole to the other in this study. Accounting for the similarity, the simplicity and the conservativeness, it is possible to use θ_{he} calculated by the 2D heat equation instead of G_{3p} in equation (17), (21) and (22) to evaluate m_{TAS} and m_{IES}.

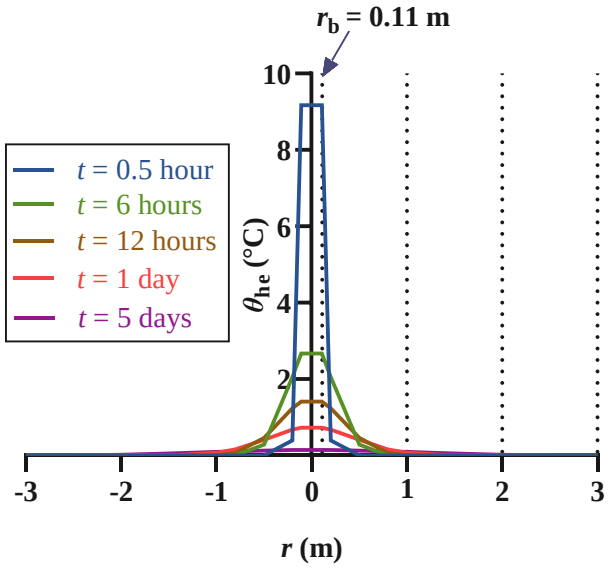

Figure 12: The heat propagation calculated by the 2D heat equation

As abovementioned, the heat transfer process of a borehole is under a constant heat flux q during each timestep. Using the 2D heat equation, the wall temperature variation of borehole j considering all the effects of the boreholes (each borehole under a line heat source of a constant initial unit of heat flux) located at distance category n and timestep m can be calculated by:

$$\theta_{\mathrm{he},j}(r_n, t_m) = \sum_{k=1}^{m} \frac{\exp\left(-\frac{{r_n}^2}{4t_k\alpha_s}\right)}{4\alpha_s\pi t_k} \cdot N_{j,n} \tag{26}$$

Combining equation (17) with equation (26), $m_{\mathrm{IES}}(j,n)$ is the first timestep that satisfies the following condition:

$$\frac{\sum_{i=1}^{n} \theta_{\mathrm{he},j}(r_i, t_{m_{\mathrm{IES}}(j,n)})}{\sum_{i=1}^{N_d} \theta_{\mathrm{he},j}(r_i, t_{m_{\mathrm{IES}}(j,n)})} < 1 - \varepsilon_{\mathrm{IES}} \tag{27}$$

Then $m_{\mathrm{IES}}(n)$ can be determined by equation (19).

As explained in the TAS method, $m_{\mathrm{TAS}}(p,n)$ is determined by the following steps:

1. Determine $m_{\mathrm{TAS,dc}}(p,n)$ by:

$$\frac{\theta_{\mathrm{he},1}\left(r_n, t_{m_{\mathrm{TAS,dc}}(p,n)+l_p}\right) - \theta_{\mathrm{he},1}\left(r_n, t_{m_{\mathrm{TAS,dc}}(p,n)}\right)}{\left(\theta_{\mathrm{he},1}\left(r_n, t_{m_{\mathrm{TAS,dc}}(p,n)+l_p}\right) + \theta_{\mathrm{he},1}\left(r_n, t_{m_{\mathrm{TAS,dc}}(p,n)}\right)\right)/2} < \varepsilon_{\mathrm{TAS}} \tag{28}$$

2. Determine $m_{\mathrm{TAS,bh}}(p,n)$ by the following equation and equation (23):

$$\frac{\sum_{n=1}^{N_\mathrm{d}} \theta_{\mathrm{he},j}\left(r_n, t_{m_{\mathrm{TAS,bh}}(p,j)+l_p}\right) - \sum_{n=1}^{N_\mathrm{d}} \theta_{\mathrm{he},j}\left(r_n, t_{m_{\mathrm{TAS,bh}}(p,j)}\right)}{\left(\sum_{n=1}^{N_\mathrm{d}} \theta_{\mathrm{he},j}\left(r_n, t_{m_{\mathrm{TAS,bh}}(p,j)+l_p}\right) + \sum_{n=1}^{N_\mathrm{d}} \theta_{\mathrm{he},j}\left(r_n, t_{m_{\mathrm{TAS,bh}}(p,j)}\right)\right)/2} < \varepsilon_{\mathrm{TAS}} \tag{29}$$

3. Determine $m_{\mathrm{TAS}}(p,n)$ by equation (24).

Using m_{TAS} and m_{IES} calculated by equation (27), (28) and (29), $G_{3\mathrm{p}}$ is calculated sooner and more often than needed, ensuring accuracy.

Equation (26) can be easily solved due to its simple mathematical form. Thus, the proposed method can quickly calculate m_{TAS} and m_{IES}, and afterwards the calculation time of $G_{3\mathrm{p}}$ will be largely reduced.

3.8 Summary of the proposed model

The fast calculation model for the thermal response factor of a large-scale boreholes GHE is shown in Figure 13. It contains four main steps:

1. Convert the field into distance categories

The N_d distance categories and their radial distances r_n (n varying from 1 to N_d) are identified from the position of borehole 1 (top left borehole). The number of times each distance category $N_{j,n}$ occurs is then evaluated for each borehole in the field.

2. Calculate the 2D heat equation

$\theta_{he,j}$ is calculated for each distance category and all timesteps by applying equation (26) to all boreholes.

3. Determine the simplification timesteps m_{TAS} and m_{IES}

According to the results of step 2, equations (19) and (27) are used to obtain $m_{IES}(n)$ for all N_n distance categories. Equations (24), (28) and (29) are used to obtain $m_{TAS}(p,n)$ for each averaging period p and each distance category n.

4. Calculate the thermal response factor

x_{dis} is firstly calculated by equation (8) to be used in the three-points method. Based on the results of step 3, G_{3p}, $G_{3p,borehole}$ and $G_{3p,GHE}$ are calculated by equations (9), (11) and (12), respectively, for all distance categories and all timesteps.

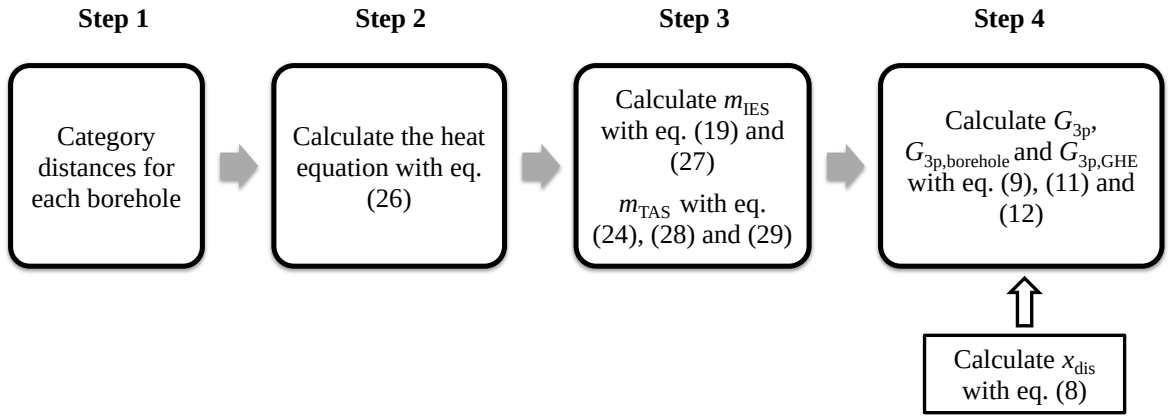

Figure 13: The flow chat of the global model for fast calculation of the thermal response factors

4 . Results and discussion

4.1 Case study

In order to deal with the long-time operation of 20 years, one year in this paper contains 8 766 hours ((365 × 3 + 366) × 24 / 4), considering the leap year. The total number of timesteps is 175 320.

The 676 boreholes contribute to 294 distance categories as shown in Figure 14. Distance category 1 has the smallest radial distance $r = r_b = 0.11$ m, and the largest radial distance r_{294} is between the first and last borehole (the diagonal of the square field) which equals to $\sqrt{(25B)^2 + (25B)^2} = 141.42$ m. Then $N_{j,n}$ is evaluated for all N_b boreholes.

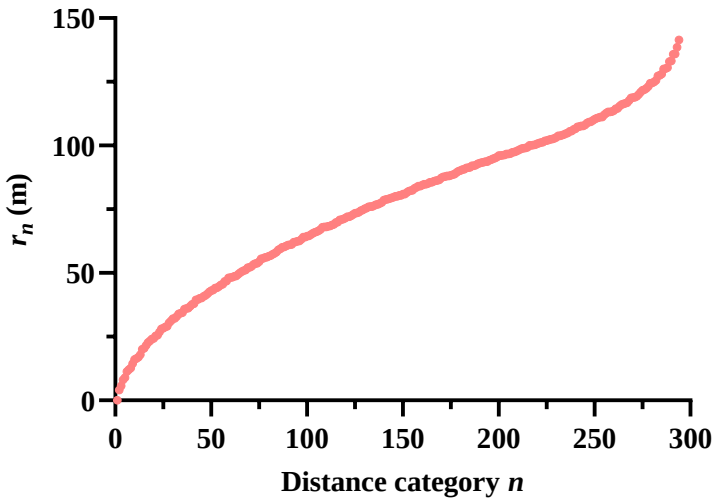

Figure 14: The distance categories and their radial distances

Four representative boreholes are chosen: top left corner borehole (borehole 1), top right corner borehole (borehole 13), bottom right corner borehole (borehole 325) and centre borehole (borehole 163) of the left top 1/4 field, as presented in Figure 15. The numbers of boreholes at different radial distance for these four boreholes are shown in Figure 16.

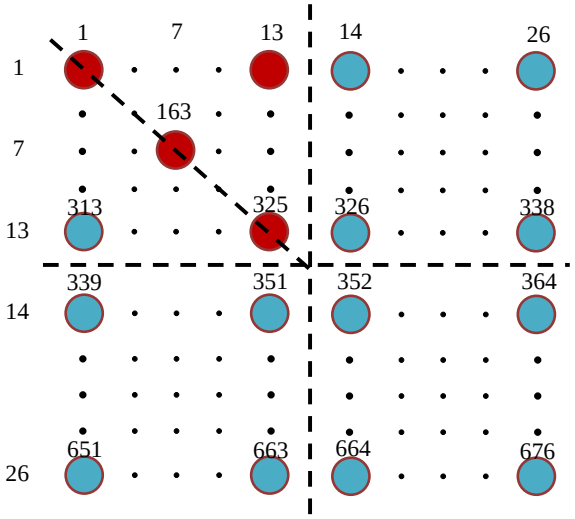

Figure 15: Four representative boreholes in the 26 × 26 square borehole field

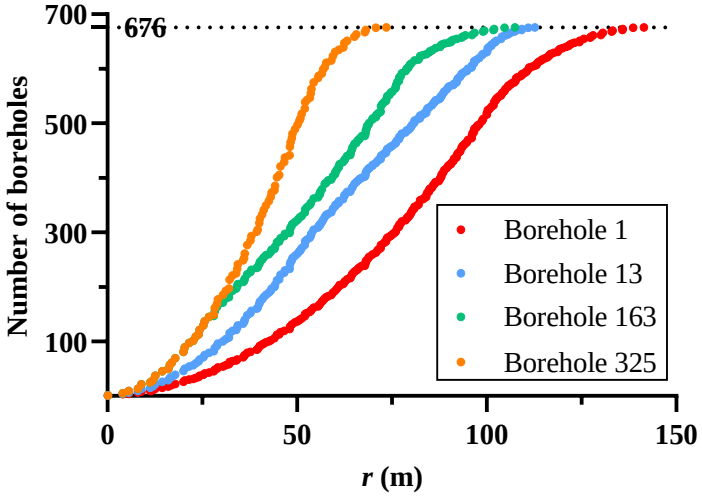

Figure 16: Number distribution of boreholes at a certain radial distance for borehole 1, 13, 163 and 325

m_{IES} for each distance category is calculated and shown in Figure 17. It can be inferred that distance category 1 starts to have an effect from the first timestep. m_{IES} increases with the radial distance. When distance category is 210 (r_{210} = 98.06 m), m_{IES} is 174 809, which means that the effect of the boreholes at distance category 210 only need to be considered from timestep 174 809 onwards. It should be noted that the total number of timesteps for 20 years is 175 320; all the boreholes at distance categories from 211 to the last distance category 294 have negligible effects on the calculated borehole, so the thermal response factor of this part does not need to be evaluated, and calculation time can be massively saved.

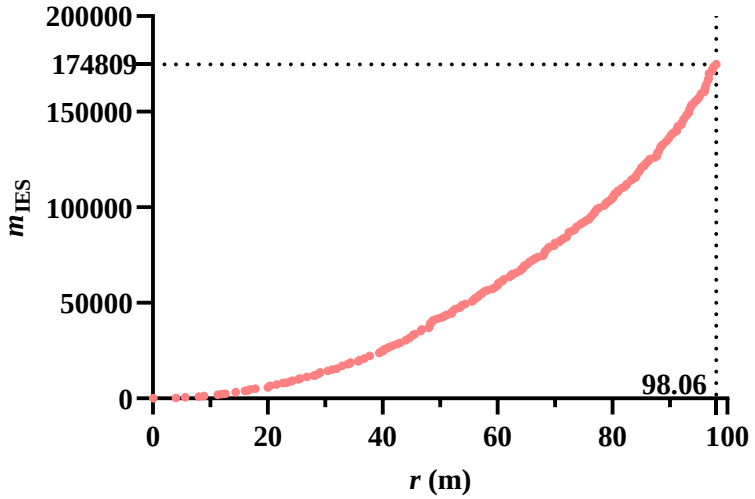

Figure 17: m_{IES} of different radial distances for 20 years operation

Figure 18 shows m_{TAS} for different distance categories. For r_1, from timestep 1 to $m_{TAS}(1,1) = 53$, G_{3p} is calculated every timestep; from timestep $m_{TAS}(1,1) + 1 = 54$ to $m_{TAS}(2,1) = 93$, G_{3p} is evaluated every 2 timesteps. From timestep $m_{TAS}(141,1) = 21\,377$ to the last timestep 175 320, G_{3p} only needs to be determined every $l_p = 1\,060$ timesteps (around 44 days). For a certain averaging range, m_{TAS} increases with the radial distance. For the largest distance category 294, the largest m_{TAS} is 172 955 for $p = 135$, and the corresponding l_p equals to 976. This means from timestep 172 955 to the last timestep 175 320, G_{3p} is calculated every 976 timesteps (around 40.6 days).

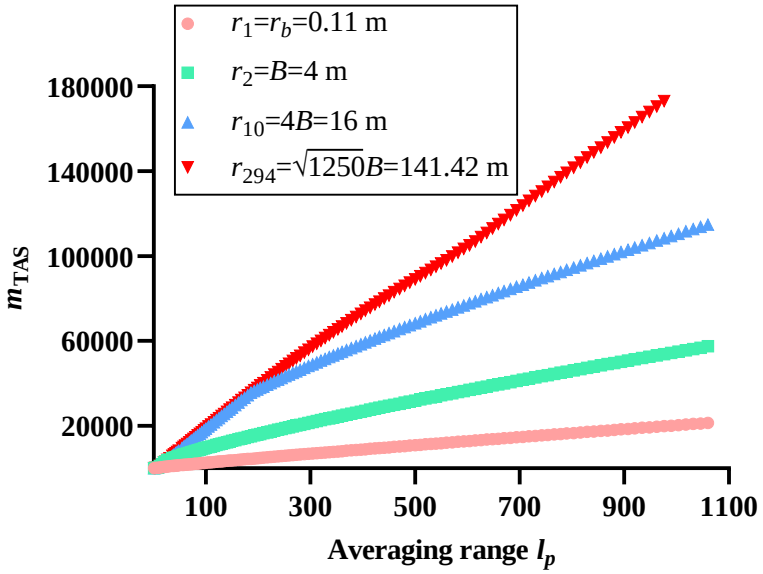

Figure 18: m_{TAS} of each averaging range at distance category 1, 2, 10 and 294

4.2 Three-points method validation

The three-points method is validated by comparing the results from the double-integration method. It focuses on the accuracy of the three-points method and does not incorporate abovementioned simplifications. The relative differences of G between the three-points and the double-integration methods (i.e. $(G_{3p}\text{-}G_{2i})/G_{2i}$) for different radial distances r are shown in Figure 19 (a) for short periods (below one year) and Figure 19 (b) for long periods (above one year), as well as those of the middle-point method (i.e. $(G_m\text{-}G_{2i})/G_{2i}$). It can be inferred that both methods are accurate for short periods, with a maximal relative difference under 6%. However the three-points method shows a better accuracy for long periods. The maximal relative difference is maintained under 4 % by the three-

points method, instead of 34 % by the middle-point method. The three-points method shows good accuracy in the calculation of *G*. Figure 20 (a) indicates the borehole wall temperature difference under the effect of another borehole between using the three-points method and the double-integration method (as reference). All the absolute temperature differences remain below 0.03 °C, which is an improvement compared to over 0.2 °C for t = 25 years by the middle-point method in Figure 4 (a). For large-scale boreholes fields, this improvement is more significant. The wall temperature differences of the corner borehole and the centre borehole in different fields between two methods are shown in Figure 20 (b) and Figure 20 (c) respectively. The absolute difference increases with the size of the borehole field and are all below 0.6 °C for the corner borehole and 1.5°C for the centre borehole for different times. This is a significant improvement compared to over 12.5 °C by the middle-point method in Figure 4 (b) and over 36 °C in Figure 4 (c). The small differences prove that the three-points method is a valid method to replace the double-integration method, meanwhile its single-integration form makes it very fast and easily computed.

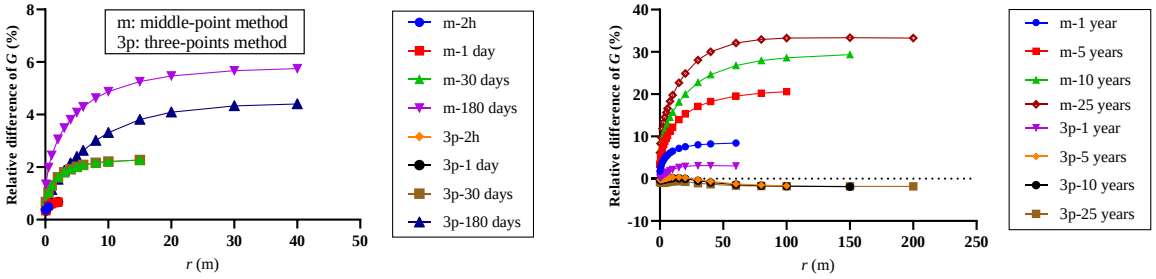

Figure 19: Relative difference of G between the three-points/middle-point method and the double-integration method for (a) short periods (below one year) (b) long periods (above one year)

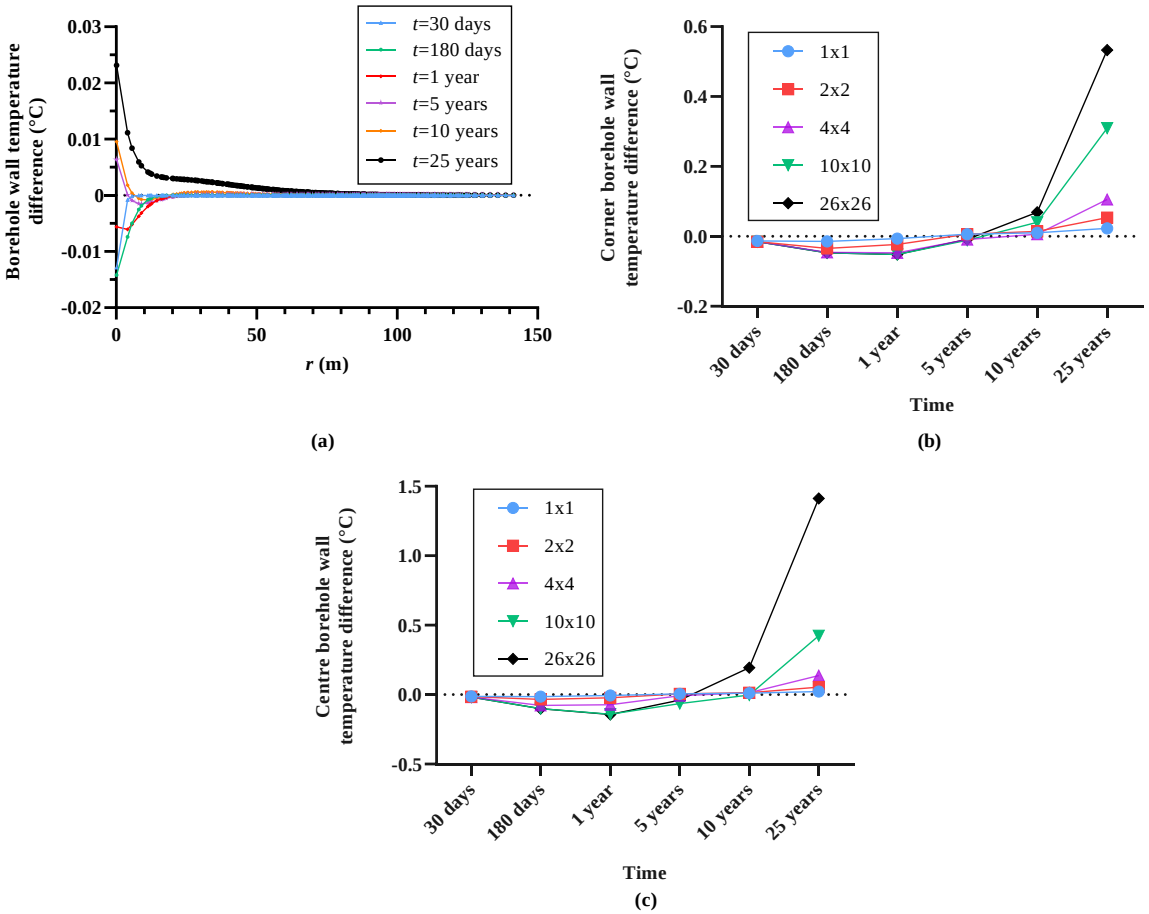

Figure 20: (a) The borehole wall temperature difference under the effect of a single borehole located at radial distance r and the borehole wall temperature difference (b) for the corner borehole and (c) for the centre borehole in a field with different sizes between the three-points method and the double-integration method (as reference)

4.3 Model validation

This subsection aims at validating the proposed model including all the simplifications. This study focuses on multi-year simulation, however it is very difficult to obtain experimental data for such a long duration. Therefore, this paper compares the thermal response factors calculated by the proposed model with the original FLS model (validated by another study [59] for long operation time) with double integration not involving any simplification, which is considered as an accurate reference. More exactly, the three thermal response factors G_{3p}, $G_{3p,borehole}$ and $G_{3p,GHE}$ of the case study were compared to G_{2i}, $G_{2i,borehole}$ and $G_{2i,GHE}$. As abovementioned, G_{3p} gives the thermal response of one borehole wall caused by another borehole located at a certain radial distance at a certain time, $G_{3p,borehole}$ gives the thermal response of one borehole wall caused by all boreholes in the field at a certain time, and $G_{3p,GHE}$ gives the thermal response of the whole GHE at a certain time.

The differences of the borehole wall temperature caused by G_{3p} and G_{2i} (as reference) for distance categories 1, 2, 10, and 100 during 20 years of operation are shown in Figure 21 every 5 000 timesteps. The absolute differences are all under 0.03 °C, at the borehole radius ($r = r_b = 0.11$ m) during during 20 years of operation. The differences reduce with the radial distance. For $r = 4$ m, $r = 16$ m and $r = 64.5$ m, the absolute differences are smaller than 0.009 °C, 0.003 °C and 0.002 °C, respectively. Therefore, the proposed method shows an excellent accuracy for the evaluation of G. The relative differences of $G_{3p,borehole}$ (i.e. $(G_{3p,borehole}-G_{2i,borehole})/G_{2i,borehole}$) for borehole 1, 13, 163 and 325 are shown in Figure 22 every 500 timesteps. All absolute relative differences are below 2 %, so it can be inferred that the proposed global model can give an accurate result for the temperature response of each borehole considering all the effects of the boreholes in the GHE field. Regarding the thermal

response factor of the whole GHE, the relative differences (i.e. ($G_{3p,GHE}$-$G_{2i,GHE}$)/$G_{2i,GHE}$ and ($G_{m,GHE}$-$G_{2i,GHE}$)/$G_{2i,GHE}$)every 500 timesteps are shown in Figure 23. The relative difference between $G_{m,GHE}$ and $G_{2i,GHE}$ reaches 23 %. However the relative difference of $G_{3p,GHE}$ is smaller than 1.5 %, indicating that the proposed model shows a better accuracy to predict the thermal response of the whole GHE as well.

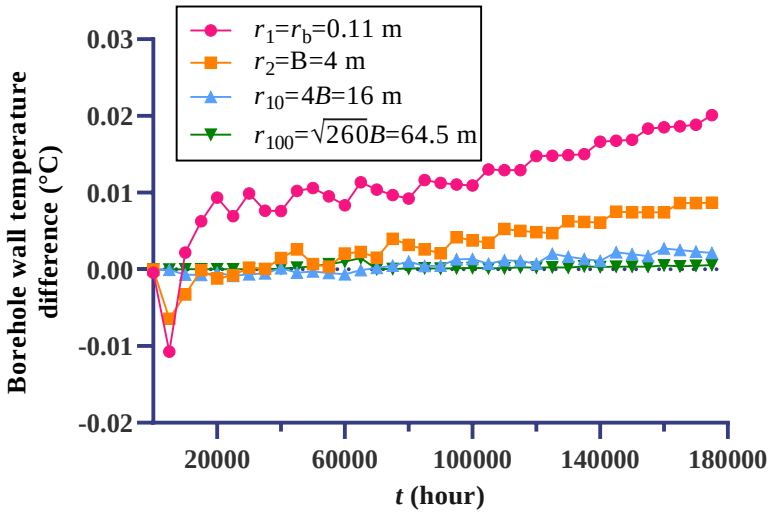

Figure 21: Temperature differences of the borehole wall caused by G_{3p} and G_{2i} (as reference) for distance category 1, 2, 10, and 100 during 20 years of operation

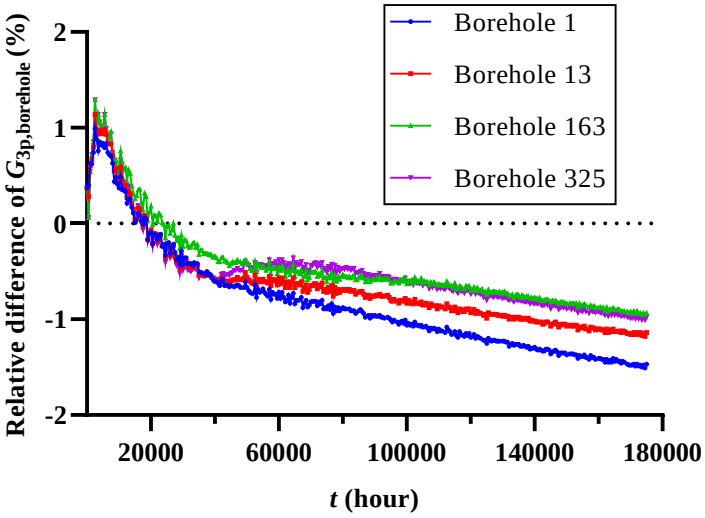

Figure 22: Relative differences of $G_{3p,borehole}$ for borehole 1, 13, 163 and 325 during 20 years of operation compared to $G_{2i,borehole}$

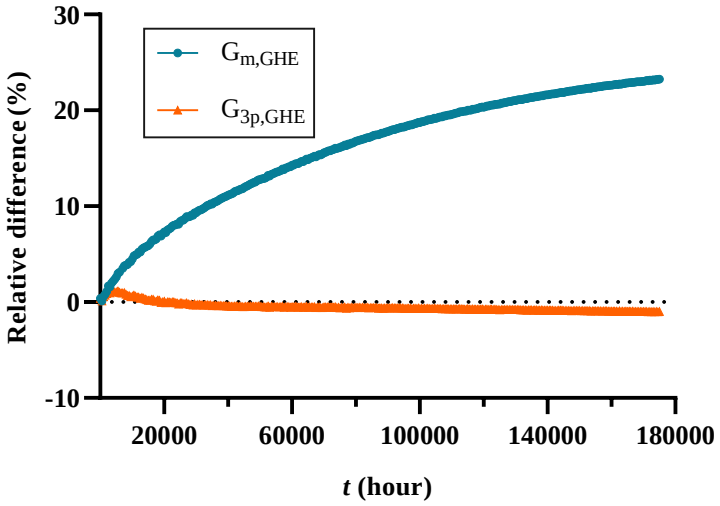

Figure 23: Relative differences of $G_{3p,GHE}$ and $G_{m,GHE}$ during 20 years of operation compared to $G_{2i,GHE}$

4.4 Calculation speed

The calculation time of the proposed model was compared to different calculation methods to analyse the calculation time reduction ability for the three main steps: distance category simplification, the three-points method and the initial effect simplification/time averaging simplification. The double-integration method without distance categories uses equation (5). The double-integration method with distance categories uses the form of equation (11) in which G_{3p} is replaced by G_{2i}. The three-points method with distance categories uses equation (11), without the initial effect/time averaging simplification. The proposed global model includes all the simplification methods. The calculation time of different methods is shown in Table 2. All methods were calculated in Matlab using a computer with an Intel i7-6700 CPU and 16 GB RAM. In the proposed model, the parallel computing with 4 computer threads were used. This could be adjusted based on the computer characteristics and the limit set by Matlab. Its simulation time with and without parallel computing was also investigated. It should be noted that the values of ε_{IES} and ε_{TAS}, which are set to 0.5 % in this paper, influence the calculation time. The larger they are, the faster the calculation is, with the sacrifice of the accuracy.

Considering that the double-integration method without distance categories method is heavily time consuming, it is only possible to measure the calculation time for short simulated periods. It cost 1.4 hours in Matlab to simulate 10 hours of operation. Since the calculation time is linear to the simulated period for this double-integration method, it was estimated that it would take almost 50 days to simulate 1 year. By applying distance category simplification to this method, the calculation time was significantly reduced to 1.7 hours, showing a calculation time reduction factor (CTRF) of approximately 700. The three-points method with distance categories cost 0.68 hour for 1 year simulated period, and it contributed to a CTRF of 2.5 compared to the double-integration method with distance categories. The proposed global model only cost 4 seconds without parallel computing for 1 year simulated period, which meant the initial effect simplification and time averaging simplification gave a CTRF of 600. The parallel computing gave a CTRF of around 2. For 1 year simulated period, the overall CTRF of the proposed model with parallel computing was around 1 000 000 compared to the double-integration method without distance categories, which was a huge improvement. Only 4 seconds of calculation time for a large-scale field of 26 × 26 boreholes for 1 year of operation makes it appropriate to simulate GHE systems in BES tools, especially in the design phase for buildings or vertical ground source heat pumps. Moreover, considering a long operation time of a GHE can be interesting. The proposed model cost about 1 minute with parallel computing and 2 minutes without parallel computing to simulate 20 years of operation, compared to nearly 1 000 days by the double-integration method without distance categories, corresponding to a CTRF of around 1 600 000 and 760 000, respectively.

The calculation time of the proposed model using double-integration instead of the three-points method was also investigated. It cost 1.5 minutes and almost 4 minutes to simulate 1 year and 20 years respectively. It shows that by applying the three-points method in the initial effect simplification/time averaging simplification can give higher CTRFs, which are 24 for one year, 8.9 for 10 years and 4.4 for 20 years simulated period. Thus, the three-points method can further increase the calculation ability, and maintain high accuracy at the same time.

Table 2: Calculation time reduction of the proposed model for a 26 × 26 borehole field

	Calculation time					
Simulated period	**Double-integration method without distance categories (estimated)**	**Double-integration method with distance categories**	**Three-points method with distance categories**	**Proposed method with parallel computing using double-integration method**	**Proposed model without parallel computing (3P method)**	**Proposed model with parallel computing (3P method)**
1 year	50 days	1.7 hours	0.68 hours	96 seconds	4 seconds	4 seconds
5 years	250 days	8.4 hours	3.4 hours	150 seconds	18 seconds	11 seconds
10 years	500 days	16.8 hours	6.9 hours	204 seconds	40 seconds	23 seconds
20 years	1000 days	33.5 hours	12.9 hours	230 seconds	114 seconds	53 seconds

It should be noted that, although the proposed model is presented with a square field configuration, it is also suitable for other configurations such as L-shaped, box-shaped, U-shaped and even irregular. The distance category simplification can be applied to other configurations but the CTRF will vary depending on the shape of the field. The initial effect simplification/time averaging simplification only considers the distance categories, thus it can still simplify the calculation after the various configurations are converted into distance categories. The proposed model can be therefore widely adapted to engineering cases and BES tools.

4.5 Discussion

The three-points method is an effective method to reduce the calculation time, since it can provide a CTRF of around 2.5 in this case study. It should be noted that our proposed model could still provide fast calculation even if it is replaced by the double-integration method.

The idea of using the 2D heat conduction equation to simplify the calculation has several advantages:

- It is an analytical approach that can easily be integrated in a BES tool.
- It is load-independent. It focuses on the evaluation of the thermal response factor (G), therefore it avoids the presence of the heating load. The calculation can be done in a stand-alone tool (Matlab in this study). Besides, the heating load signal is fully respected in our model, avoiding the reshaping procedure presented in the load-aggregation algorithm [36] which might lead to inaccuracy. This is very important and convenient for the integration in the BES tool, which gives the building load at every timestep (one hour or smaller).
- The values of G can be used as an input table to the BES tool. When dealing with the temperature calculation, e.g. equation (11), the varying load and thermal interactions could be evaluated by reading this table. The coupling between varying load and G becomes a basic computation, which is rather straightforward and fast for most tools.
- This simplification is easy, accurate and fast, avoiding complex mathematical algorithms, such as the FFT method [43].

This article focuses on the uniform heating load distribution to each borehole, which can help to reduce the mathematic complexity. As abovementioned, the proposed model could also be applied to

non-uniform distribution, because the core of the simplification based on the 2D heat conduction is load-independent. However this would require some adjustments such as in equation (11) in which, due to the non-uniform distribution, there will be different weighting factors determined by different loads for each G_{3p}, instead of identical ones in the uniform distribution.

This study did not consider the simplification of the temporal superposition (load history), because normally it is easy and fast for a tool to deal with this mathematical problem, if G of the whole field is known. Besides, it is much easier to integrate the GHE model in the BES tools which directly generates the loads.

One limit of this study is that it focuses on the uniform heating load distribution to each borehole, which can help to reduce the mathematic complexity. However, as abovementioned, the proposed model could also be applied to non-uniform distribution, because the core of the simplification based on the 2D heat conduction is load-independent. This would require some adjustments such as in Eq. (11) in which, due to the non-uniform distribution, there will be different weighting factors determined by different loads for each G3p, instead of identical ones in the uniform distribution. Since this work is based on the original FLS model, they share some common limits e.g. a constant heat flux along the depth of the borehole and the neglect of ground water movement. Homogeneous layer with constant thermophysical properties is another limit which can be refined by considering multi-layers with different properties. Integrating the improvements on these limits with our model is another perspective.

5 . Conclusion

The optimisation of the design and operation of large-scale boreholes heat exchangers for long operation time brings massive calculation regarding the thermal response factor G of the GHE field. middle-point temperature. This article presents a global model to quickly and accurately evaluate G, combining the FLS model, the 2D heat conduction equation, and a newly developed three-points method.

The three-points method is introduced to determine the representative borehole wall temperature. It considers three points located at the top, middle and bottom of the borehole and uses the average of these three points to represent the borehole wall temperature, avoiding the non-negligible errors of using the borehole middle-point temperature for long operation time. The results show that the relative differences of G between the proposed method and the double-integration method are below 5 % for all cases. The absolute wall temperature difference of the corner borehole of a 26 × 26 field is below 0.4 °C compared to over 12.5 °C by the middle-point method for a simulated time of 25 years. Besides its good accuracy, this method remains in the form of a single integration to keep a reasonable computation time. In addition, the position determination equation can be applied to different borehole configurations due to its universality.

In the global model, the first step is to sort the large number of boreholes in increasing distance categories. In the second step, the 2D heat conduction equation determines when interactions between boreholes are negligible and when detailed calculations are needed. In the third step, the 2D heat conduction equation evaluates how often the interactions have to be recalculated. In the last step, the thermal response factors are computed by the three-points method. An example of a 26 × 26 square borehole matrix is studied in this paper. The results show that the proposed model can give accurate results for G_{3p} (smaller than 5 %), $G_{3p,borehole}$ and $G_{3p,GHE}$ (smaller than 2 %), meanwhile the calculation time for one simulated year decreases by a factor of around 1 000 000 to only 4 seconds comparing to the double-integration method without any simplification. In this case, simulating 20 years of operation only requires 1 minute. The proposed model is suitable not only for a square borehole configuration, but also for other configurations such as L-shaped, box-shaped, U-shaped and even irregular. Its universality, accuracy, load-independency and calculation speed facilitate its integration into building energy simulation tools to optimise the design and operation of GCHP systems.

Acknowledgement

The authors would like to thank the financial support by China Scholarship Council (CSC) and the Chair ParisTech VINCI Eco-design of buildings and infrastructure.

Reference

[1] Ikeda S, Choi W, Ooka R. Optimization method for multiple heat source operation including ground source heat pump considering dynamic variation in ground temperature. Applied Energy 2017;193:466–78. https://doi.org/10.1016/j.apenergy.2017.02.047.

[2] Wang H, Liu B, Yang F, Liu F. Test investigation of operation performance of novel split-type ground source heat pump systems for clean heating of rural households in North China. Renewable Energy 2021;163:188–97. https://doi.org/10.1016/j.renene.2020.08.147.

[3] Gultekin A, Aydin M, Sisman A. Effects of arrangement geometry and number of boreholes on thermal interaction coefficient of multi-borehole heat exchangers. Applied Energy 2019;237:163–70. https://doi.org/10.1016/j.apenergy.2019.01.027.

[4] Zanchini E, Jahanbin A. Simple equations to evaluate the mean fluid temperature of double-U-tube borehole heat exchangers. Applied Energy 2018;231:320–30. https://doi.org/10.1016/j.apenergy.2018.09.094.

[5] Yang H, Cui P, Fang Z. Vertical-borehole ground-coupled heat pumps: A review of models and systems. Applied Energy 2010;87:16–27. https://doi.org/10.1016/j.apenergy.2009.04.038.

[6] Chen Y, Pan B, Zhang X, Du C. Thermal response factors for fast parameterized design and long-term performance simulation of vertical GCHP systems. Renewable Energy 2019;136:793–804. https://doi.org/10.1016/j.renene.2018.12.114.

[7] Cimmino M. Fast calculation of the g-functions of geothermal borehole fields using similarities in the evaluation of the finite line source solution. Journal of Building Performance Simulation 2018;11:655–68. https://doi.org/10.1080/19401493.2017.1423390.

[8] Priarone A, Fossa M. Temperature response factors at different boundary conditions for modelling the single borehole heat exchanger. Applied Thermal Engineering 2016;103:934–44. https://doi.org/10.1016/j.applthermaleng.2016.04.038.

[9] Fossa M, Priarone A. Constant temperature response factors for fast calculation of sparse BHE field g-functions. Renewable Energy 2019;131:1236–46. https://doi.org/10.1016/j.renene.2018.07.136.

[10] Fossa M, Priarone A, Silenzi F. Superposition of the single point source solution to generate temperature response factors for geothermal piles. Renewable Energy 2020;145:805–13. https://doi.org/10.1016/j.renene.2019.05.011.

[11] Eskilson P. Thermal analysis of heat extraction boreholes. 1987.

[12] Yu M, Ma T, Zhang K, Cui P, Hu A, Fang Z. Simplified heat transfer analysis method for large-scale boreholes ground heat exchangers. Energy and Buildings 2016;116:593–601. https://doi.org/10.1016/j.enbuild.2016.02.001.

[13] Yang Y, Li M. Short-time performance of composite-medium line-source model for predicting responses of ground heat exchangers with single U-shaped tube. International Journal of Thermal Sciences 2014;82:130–7. https://doi.org/10.1016/j.ijthermalsci.2014.04.002.

[14] Naldi C, Zanchini E. A new numerical method to determine isothermal g-functions of borehole heat exchanger fields. Geothermics 2019;77:278–87. https://doi.org/10.1016/j.geothermics.2018.10.007.

[15] Kerme ED, Fung AS. Heat transfer simulation, analysis and performance study of single U-tube borehole heat exchanger. Renewable Energy 2020;145:1430–48. https://doi.org/10.1016/j.renene.2019.06.004.

[16] Yu X, Li H, Yao S, Nielsen V, Heller A. Development of an efficient numerical model and analysis of heat transfer performance for borehole heat exchanger. Renewable Energy 2020. https://doi.org/10.1016/j.renene.2020.01.044.

[17] Chwieduk M. New global thermal numerical model of vertical U-tube ground heat exchanger. Renewable Energy 2021;168:343–52. https://doi.org/10.1016/j.renene.2020.12.069.

[18] Delazar A, Hu E, Kotousov A, Sofyan SE. A novel three-dimensional implicit numerical model of a borehole field heat exchanger that accounts for seasonal fluctuations of the soil temperature. Geothermics 2021;97:102236. https://doi.org/10.1016/j.geothermics.2021.102236.

[19] Zhang F, Fang L, Jia L, Man Y, Cui P, Zhang W, et al. A dimension reduction algorithm for numerical simulation of multi-borehole heat exchangers. Renewable Energy 2021;179:2235–45. https://doi.org/10.1016/j.renene.2021.08.028.

[20] Zarrella A, Scarpa M, De Carli M. Short time step analysis of vertical ground-coupled heat exchangers: The approach of CaRM. Renewable Energy 2011;36:2357–67. https://doi.org/10.1016/j.renene.2011.01.032.
[21] Li M, Lai ACK. Review of analytical models for heat transfer by vertical ground heat exchangers (GHEs): A perspective of time and space scales. Applied Energy 2015;151:178–91. https://doi.org/10.1016/j.apenergy.2015.04.070.
[22] Ingersoll LR, Plass HJ. Theory of the ground pipe heat source for the heat pump. ASHRAE Transactions 1948;54:339–48.
[23] Zeng HY, Diao NR, Fang ZH. A finite line-source model for boreholes in geothermal heat exchangers. Heat Trans Asian Res 2002;31:558–67. https://doi.org/10.1002/htj.10057.
[24] Deerman JD, Kavanaugh SP. Simulation of vertical U-tube ground-coupled heat pump systems using the cylindrical heat source solution. ASHRAE Transactions 1991;97:287–95.
[25] Li M, Lai ACK. New temperature response functions (G functions) for pile and borehole ground heat exchangers based on composite-medium line-source theory. Energy 2012;38:255–63. https://doi.org/10.1016/j.energy.2011.12.004.
[26] Li M, Li P, Chan V, Lai ACK. Full-scale temperature response function (G-function) for heat transfer by borehole ground heat exchangers (GHEs) from sub-hour to decades. Applied Energy 2014;136:197–205. https://doi.org/10.1016/j.apenergy.2014.09.013.
[27] Zhang L, Zhang Q, Huang G. A transient quasi-3D entire time scale line source model for the fluid and ground temperature prediction of vertical ground heat exchangers (GHEs). Applied Energy 2016;170:65–75. https://doi.org/10.1016/j.apenergy.2016.02.099.
[28] Abdelaziz SL, Ozudogru TY, Olgun CG, Martin JR. Multilayer finite line source model for vertical heat exchangers. Geothermics 2014;51:406–16. https://doi.org/10.1016/j.geothermics.2014.03.004.
[29] Rivera JA, Blum P, Bayer P. A finite line source model with Cauchy-type top boundary conditions for simulating near surface effects on borehole heat exchangers. Energy 2016;98:50–63. https://doi.org/10.1016/j.energy.2015.12.129.
[30] Guo Y, Hu X, Banks J, Liu WV. Considering buried depth in the moving finite line source model for vertical borehole heat exchangers—A new solution. Energy and Buildings 2020;214:109859. https://doi.org/10.1016/j.enbuild.2020.109859.
[31] Zhou Y, Wu Z, Wang K. An analytical model for heat transfer outside a single borehole heat exchanger considering convection at ground surface and advection of vertical water flow. Renewable Energy 2021;172:1046–62. https://doi.org/10.1016/j.renene.2021.03.102.
[32] Zhang X, Zhang T, Jiang Y, Li B. Improvement on an analytical finite line source model considering complex initial and boundary conditions: Part 1, model development and validation. Energy and Buildings 2019;198:1–10. https://doi.org/10.1016/j.enbuild.2019.05.011.
[33] Lamarche L, Beauchamp B. A new contribution to the finite line-source model for geothermal boreholes. Energy and Buildings 2007;39:188–98. https://doi.org/10.1016/j.enbuild.2006.06.003.
[34] Koohi-Fayegh S, Rosen MA. An analytical approach to evaluating the effect of thermal interaction of geothermal heat exchangers on ground heat pump efficiency. Energy Conversion and Management 2014;78:184–92. https://doi.org/10.1016/j.enconman.2013.09.064.
[35] Zhang C, Wang Y, Liu Y, Kong X, Wang Q. Computational methods for ground thermal response of multiple borehole heat exchangers: A review. Renewable Energy 2018;127:461–73. https://doi.org/10.1016/j.renene.2018.04.083.
[36] Yavuzturk C, Spitler J. A short time step response factor model for vertical ground loop heat exchangers. ASHRAE Transactions 1999;105.
[37] Cullin JR, Spitler JD. A computationally efficient hybrid time step methodology for simulation of ground heat exchangers. Geothermics 2011;40:144–56. https://doi.org/10.1016/j.geothermics.2011.01.001.
[38] Bernier M, Pinel P, Labib R, Paillot R. A multiple load aggregation algorithm for annual hourly simulations of GCHP systems. HVAC&R Research 2004;10:471–87. https://doi.org/10.1080/10789669.2004.10391115.
[39] Claesson J, Javed S. A load-aggregation method to calculate extraction temperatures of borehole heat exchangers. ASHRAE Transactions 2012;118:530–9.

[40] Mitchell MS, Spitler JD. Characterization, testing, and optimization of load aggregation methods for ground heat exchanger response-factor models. Science and Technology for the Built Environment 2019;25:1036–51. https://doi.org/10.1080/23744731.2019.1648936.
[41] Lamarche L, Beauchamp B. A fast algorithm for the simulation of GCHP systems. ASHRAE Transactions 2007;113 PART 1:470–6.
[42] Lamarche L. A fast algorithm for the hourly simulations of ground-source heat pumps using arbitrary response factors. Renewable Energy 2009;34:2252–8. https://doi.org/10.1016/j.renene.2009.02.010.
[43] Zhang L, Huang G, Zhang Q, Wang J. An hourly simulation method for the energy performance of an office building served by a ground-coupled heat pump system. Renewable Energy 2018;126:495–508. https://doi.org/10.1016/j.renene.2018.03.082.
[44] Marcotte D, Pasquier P. Fast fluid and ground temperature computation for geothermal ground-loop heat exchanger systems. Geothermics 2008;37:651–65. https://doi.org/10.1016/j.geothermics.2008.08.003.
[45] Katsura T, Nagano K, Takeda S. Method of calculation of the ground temperature for multiple ground heat exchangers. Applied Thermal Engineering 2008;28:1995–2004. https://doi.org/10.1016/j.applthermaleng.2007.12.013.
[46] Zhang D. Research into heat exchange between wells of the U-tube ground heat exchanger. PhD thesis. Southwest Jiaotong University, 2010.
[47] Kurevija T, Vulin D, Krapec V. Effect of borehole array geometry and thermal interferences on geothermal heat pump system. Energy Conversion and Management 2012;60:134–42. https://doi.org/10.1016/j.enconman.2012.02.012.
[48] Teza G, Galgaro A, De Carli M. Long-term performance of an irregular shaped borehole heat exchanger system: Analysis of real pattern and regular grid approximation. Geothermics 2012;43:45–56. https://doi.org/10.1016/j.geothermics.2012.02.004.
[49] Beck M, Bayer P, de Paly M, Hecht-Méndez J, Zell A. Geometric arrangement and operation mode adjustment in low-enthalpy geothermal borehole fields for heating. Energy 2013;49:434–43. https://doi.org/10.1016/j.energy.2012.10.060.
[50] Cimmino M, Bernier M. A semi-analytical method to generate g-functions for geothermal bore fields. International Journal of Heat and Mass Transfer 2014;70:641–50. https://doi.org/10.1016/j.ijheatmasstransfer.2013.11.037.
[51] Peuportier B, Blanc-Sommereux I. Simulation tool with its expert interface for the thermal design of multizone buildings. International Journal of Solar Energy 1990;8:109–20. https://doi.org/10.1080/01425919008909714.
[52] Hein P, Kolditz O, Görke U-J, Bucher A, Shao H. A numerical study on the sustainability and efficiency of borehole heat exchanger coupled ground source heat pump systems. Applied Thermal Engineering 2016;100:421–33. https://doi.org/10.1016/j.applthermaleng.2016.02.039.
[53] Michopoulos A, Kyriakis N. A new energy analysis tool for ground source heat pump systems. Energy and Buildings 2009;41:937–41. https://doi.org/10.1016/j.enbuild.2009.03.017.
[54] Capozza A, Zarrella A, De Carli M. Long-term analysis of two GSHP systems using validated numerical models and proposals to optimize the operating parameters. Energy and Buildings 2015;93:50–64. https://doi.org/10.1016/j.enbuild.2015.02.005.
[55] Li M, Zhou C, Rao Z. Hourly 50-year simulations of ground-coupled heat pumps using high-resolution analytical models. Energy Conversion and Management 2019;193:15–24. https://doi.org/10.1016/j.enconman.2019.04.051.
[56] Wang G, Wang W, Luo J, Zhang Y. Assessment of three types of shallow geothermal resources and ground-source heat-pump applications in provincial capitals in the Yangtze River Basin, China. Renewable and Sustainable Energy Reviews 2019;111:392–421. https://doi.org/10.1016/j.rser.2019.05.029.
[57] Claesson J, Javed S. An analytical method to calculate borehole fluid temperatures for time-scales from minutes to decades. ASHRAE Transactions 2011;117:279–88.
[58] Wang L, Zhou X, Wei X. Heat Conduction: Mathematical Models and Analytical Solutions. Springer Science & Business Media; 2007.

[59] Bertagnolio S, Bernier M, Kummert M. Comparing vertical ground heat exchanger models. Journal of Building Performance Simulation 2012;5:369–83. https://doi.org/10.1080/19401493.2011.652175.

Nomenclature

List of abbreviations

2D	Two-dimensional
BES	Building energy simulation
COP	Coefficient of performance
CTRF	Calculation time reduction factor
FFT	Fast Fourier transform
FLS	Finite line source
GCHP	Ground coupled heat pump
GHE	Ground heat exchanger

List of symbols

$a_1 \sim a_8$	Location factor parameter
G	Thermal response factor
G_{2i}	Thermal response factor of a borehole wall temperature under the other borehole's effect using the double-integration method
$G_{2i,borehole}$	Thermal response factor of a certain borehole wall temperature under all boreholes' effect using the double-integration method
$G_{2i,GHE}$	Thermal response factor of GHE using the double-integration method
G_m	Thermal response factor of a borehole wall temperature under the other borehole's effect using the middle-point method
$G_{m,borehole}$	Thermal response factor of a certain borehole wall temperature under all boreholes' effect using the middle-point method
$G_{m,GHE}$	Thermal response factor of the GHE using the middle-point method
G_{3p}	Thermal response factor of a borehole wall temperature under the other borehole's effect using the three-points method
$G_{3p,borehole}$	Thermal response factor of a certain borehole wall temperature under all boreholes' effect using the three-points method
$G_{3p,GHE}$	Thermal response factor of GHE using the three-points method
$m_{TAS,dc}$	Averaging simplification timestep determined by the distance category
$m_{TAS,bh}$	Averaging simplification timestep determined by the borehole
n	Distance category
N_b	Number of boreholes in GHE
$N_{b,sym}$	Number of boreholes after symmetry
N_d	Number of total distance categories
$N_{j,n}$	Number of times distance category n occurs for borehole j
p	Averaging range
p_{max}	Maximal averaging range
q	Heat load per meter, W/m
$q_{i,m}$	Heat load per meter of i^{th} boreheole at timestep m, W/m
q_k	Heat load per meter of each boreheole at timestep k, W/m
Q_{GHE}	Heat load of GHE, W
r	Radial distance to the borehole centre line, m
r_b	Borehole radius, m
$r_{i,j}$	Radial distance between i^{th} boreheole and j^{th} boreheole
r_n	Radial distance of n^{th} distance category, m
t	Time, s
t_m	Time at timestep m, s
T	Temperature, °C

h	Integral variable along borehole depth	T_0	Initial ground temperature, °C
H	Borehole depth, m	T_b	Borehole wall temperature, °C
H_{bottom}	Borehole depth of bottom point in three-points method, m	$T_{b,j}$	Borehole wall temperature of the j^{th} boreheole, °C
H_{top}	Borehole depth of top point in three-points method, m	x_{dis}	Location factor
i	The i^{th} boreheole	z	Vertical coordinate of borehole, m
j	The j^{th} boreheole		
k	The k^{th} timestep	***List of Greek letters***	
l_p	Averaging range for averaging period p	α_s	Thermal diffusivity of ground, m^2/s
l_{pmax}	Averaging range for maximal averaging period p_{max}	ε_{IES}	Tolerance of initial effect simplification
m	Timestep	ε_{TAS}	Tolerance of time averaging simplification
m_{end}	End of timestep	θ_{he}	Temperature variation by heat equation, °C
m_{IES}	Initial effect simplification timestep	$\theta_{he,j}$	Temperature variation of j^{th} borehole wall by heat equation, °C
m_{TAS}	Averaging simplification timestep	λ_s	Thermal conductivity of ground, W/m.°C